A bacterial regulatory uORF senses multiple classes of ribosome-targeting antibiotics

Gabriele Baniulyte[1] and Joseph T. Wade[1,2,3,4]

[1] Department of Biomedical Sciences, School of Public Health, University at Albany, SUNY, Rensselaer, NY 12144, USA.

[2] Wadsworth Center, New York State Department of Health, Albany, NY 12208, USA.

[3] RNA Institute, University at Albany, SUNY, Albany, NY 12222, USA.

[4] Corresponding author: joseph.wade@health.ny.gov

ABSTRACT

Expression of many bacterial genes is regulated by *cis*- and *trans*-acting elements in their 5' upstream regions (URs). *Cis*-acting regulatory elements in URs include upstream ORFs (uORF), short ORFs that sense translation stress that manifests as ribosomes stalling at specific codons within the uORF. Here, we show that the transcript encoding the *Escherichia coli* TopAI-YjhQ toxin-antitoxin system is regulated by a uORF that we name "*toiL*". We propose that in the absence of translation stress, a secondary structure in the UR represses translation of the *topAI* transcript by occluding the ribosome-binding site. Translation repression of *topAI* leads to premature Rho-dependent transcription termination within the *topAI* ORF. At least five different classes of ribosome-targeting antibiotics relieve repression of *topAI*. Our data suggest that these antibiotics function by stalling ribosomes at different positions within *toiL*, thereby altering the RNA secondary structure around the *topAI* ribosome-binding site. Thus, *toiL* is a multipurpose uORF that can respond to a wide variety of translation stresses.

INTRODUCTION

Expression of many bacterial genes is regulated by elements in their upstream regions (URs) (Adams et al., 2021). UR RNA can contain binding sites for *trans*-acting factors such as regulatory RNAs or RNA-binding proteins. UR RNAs can also include *cis*-acting elements, such as sequences that form secondary structures, and short ORFs (sORFs) known as upstream ORFs (uORFs). Regulatory elements in URs can modulate transcription termination within the UR, RNase accessibility within the UR, or translation initiation of the downstream gene.

uORFs are typically <50 codons in length, and sense translational stress to regulate expression of the downstream gene. Environmental perturbations promote ribosome stalling within uORFs, often in a sequence-specific manner (Ramu et al., 2009); stalled ribosomes alter the UR RNA secondary structure, modulating the formation of transcription terminators, the accessibility of the ribosome binding site for the downstream gene, or loading sites for the Rho transcription termination factor. Ribosome stalling within uORFs can be mediated by limiting concentrations of charged tRNAs (Landick and Yanofsky, 1987), or by small molecules that bind the translating ribosomes, including amino acids and antibiotics (reviewed by (Seip and Innis, 2016)).

Translation repression mediated by regulatory elements in URs can lead to an additional level of repression at the level of transcription termination (Adams et al., 2021; Baniulyte et al., 2017; Bastet et al., 2017; Bossi et al., 2012; Yakhnin et al., 2001). This occurs because Rho-dependent transcription termination is inhibited by translation (Adhya and Gottesman, 1978; Richardson, 2002). Reduced translation mediated by regulatory elements in URs allows Rho to load onto Rho utilization (Rut) sequences in the nascent RNA for the ORF that would otherwise be occluded by ribosomes. Ruts are enriched for ‘YC’ dinucleotides, lack extensive secondary structure, and have a high C:G ratio (Alifano et al., 1991; Nadiras et al., 2018; Rivellini et al., 1991; Schneider et al., 1993). The relatively low information content required for a Rut means that many sequences within ORFs can function as a Rut when translation is repressed. Translating ribosomes may also inhibit Rho termination by

preventing association of Rho with RNA polymerase (RNAP) and the associated transcription elongation factor NusG (Burmann et al., 2010).

Genome-wide studies of transcription termination *Escherichia coli* and *Mycobacterium tuberculosis* have identified many Rho termination events within ORFs (Adams et al., 2021; Cardinale et al., 2008; Dar and Sorek, 2018; D'Halluin et al., 2022; Peters et al., 2012, 2009), suggesting that modulation of premature Rho termination is a widespread regulatory mechanism. Here, we characterize the mechanism of regulated Rho termination within the *E. coli topAI* gene that is operonic with two additional genes, *yjhQ* and *yjhP* (Figure 1A) (Mao et al., 2015). The *topAI* and *yjhQ* genes encode a type II toxin-antitoxin system, where *topAI* encodes a topoisomerase A inhibitor, and *yjhQ* encodes the cognate antitoxin (Yamaguchi and Inouye, 2015). We show that Rho-dependent transcription termination within *topAI* is a consequence of translation repression. We further show that the long 5′ UR of *topAI* encodes a regulatory uORF, *toiL* (Figure 1A), that acts as a sensor for translation stress caused by multiple classes of ribosome-targeting antibiotics. We propose that these antibiotics promote ribosome stalling at various sites within *toiL*, and that ribosome stalling anywhere within *toiL* unmasks the ribosome binding site of *topAI*. Thus, *toiL* is a multipurpose regulatory uORF that can sense a wide variety of translational stresses.

RESULTS

Translational repression of *topAI* leads to intragenic Rho-dependent transcription termination

Genome-scale analysis of Rho termination identified a putative termination site in the coding region of *topAI* (Adams et al., 2021; Peters et al., 2012). The *topAI* transcript has an unusually long UR (171 nt) (Thomason et al., 2015), suggesting that Rho termination within *topAI* may be regulated by sequences in the UR. To independently assess whether Rho prematurely terminates *topAI* transcription, we constructed a *lacZ* transcriptional reporter fusion that included the *topAI* promoter and UR, and 42 nt of the *topAI* coding region (Figure 1B). We measured expression of this reporter fusion in wild-type cells and cells expressing the R66S Rho mutant that is defective for RNA binding and termination (Baniulyte et al., 2017; Martinez et al., 1996). We observed ~7-fold higher expression in *rho* mutant cells than in wild-type cells (Figure 1C), consistent with a Rho termination site upstream of position 42 of the *topAI* gene.

The precise length and position of a *rut* is difficult to predict, since Rho binds RNA with relatively low specificity; however, Rho is believed to favor pyrimidine-rich, unstructured RNA regions (Chhakchhuak et al., 2018; Nadiras et al., 2018). The most pyrimidine-rich region of the *topAI* UR is at the very 5’ end. Mutating just four C residues in the Rho-terminated construct of *topAI* (Figure 1B) caused a 4-fold increase in expression in wild-type cells, but no change in expression in *rho* mutant cells (Figure 1C). We conclude that the *rut* includes the pyrimidine-rich sequence at the very 5’ end of the *topAI* transcript.

To determine the position of the Rho termination site, we measured transcriptional activity of a “short” *topAI*::*lacZ* fusion that includes only the first 10 bp of the *topAI* ORF (Figure 1B). The effect of mutating *rho* on expression of this short reporter fusion was substantially lower than that observed for the longer reporter fusion, with no difference in expression observed for the short reporter fusion containing the mutant *rut* sequence (Figure 1C). This suggests that most of the transcription termination occurs between nucleotides 10

and 42 of the *topAI* coding region. We conclude that Rho loads onto the RNA early in the *topAI* transcript, but does not trigger termination until RNAP is within the ORF, >180 nt further downstream.

Translating ribosomes protect nascent mRNA in protein-coding regions from Rho (de Smit et al., 2009). Given that Rho termination occurs within the *topAI* ORF, we speculated that *topAI* is translationally repressed. To test whether *topAI* is actively translated, we constructed a *topAI-lux* translational reporter fusion (Figure 2A; Figure 2 – figure supplement 1A). We compared expression of this reporter fusion in wild-type and *rho* mutant cells. Although transcriptional repression of *topAI* is relieved in the *rho* mutant background (Figure 1), we observed strong repression of the *topAI-lux* translation in both wild-type and *rho* mutant cells (Figure 2 – figure supplement 1B). These data suggest that Rho termination within the *topAI* coding region is a consequence of translational repression.

topAI repression is relieved under conditions of translation stress

Translation repression often occurs by binding of a *trans*-acting factor (e.g., protein, sRNA, small molecule) overlapping the ribosome-binding site (Breaker, 2018; Kriner et al., 2016). To identify *trans*-acting regulators of *topAI*, we used a genetic selection for spontaneous mutants with increased *topAI* expression. Briefly, the mutant selection used a *topAI-lacZ* construct in a Δ*lacZ* background; overnight cultures were plated on minimal medium with lactose as the only carbon source, only allowing growth of spontaneous mutants with upregulated *topAI* expression (*cis*-acting mutants were discarded). We isolated 42 mutants with upregulated *topAI* expression. 39 of the mutants had a mutant *rho* gene (see Methods for details), suggesting that the screen was saturating. We isolated three additional mutants that each carry single base mutations in one of the seven copies of the 23S rRNA gene, in domain IV, helix 69 (*rrlA* ΔG1911, *rrlC* ΔT1917) or domain V, helix 80 (*rrlA* G2253T) (Table S1). Mutations in these regions of 23S rRNA have been suggested to cause nonsense and frameshift readthrough, defects in translation fidelity and ribosome assembly, and reduced binding of ribosome release factors (Feinberg and Joseph, 2006; Gregory et al., 1994; Hirabayashi et al., 2006; Kipper et al., 2011; Liiv et al., 2005). To test whether the rRNA mutations are sufficient to upregulate *topAI* translation, we

expressed wild-type or mutant (23S rRNA ΔT1917) rRNA operons in *trans* in an otherwise wild-type strain, and measured expression of the *topAI-lux* translational reporter fusion. For these and all additional assays of *topAI-lux* reporter fusions, we used a strain lacking *topAI* and *yjhQ*, to rule out the possibility of autoregulation. Supplying the mutant 23S rRNA in *trans* resulted in increased *topAI* expression, whereas wild-type 23S rRNA did not (Figure 2B). Thus, the 23S rRNA mutation is dominant over the seven chromosomal rRNA operons, suggesting that the effect of the mutations in 23S rRNA genes on *topAI* expression is not simply due to a reduction in levels of active ribosomes.

Expression of toxin-antitoxin genes is often induced by environmental stresses (Page and Peti, 2016). We next aimed to identify an environmental condition(s) that *topAI* responds to. Given the effect of mutating 23S rRNA on *topAI* expression, we speculated that perturbing translation with ribosome-targeting antibiotics might induce expression of *topAI*. Moreover, increases in *topAI* mRNA levels upon treatment with erythromycin or clindamycin have been reported previously (Dzyubak and Yap, 2016). We measured expression of the *topAI* translational reporter fusion in cells grown with each of 12 ribosome-targeting antibiotics at sub-inhibitory concentrations. Tetracycline, spectinomycin, retapamulin, tylosin and erythromycin caused increases in expression from 250-fold to 4,000-fold of the *topAI-lux* translational fusion (Figure 2C; Table S2). We observed no change in expression in response to treatment with chloramphenicol (Figure 2C), kasugamycin, gentamicin, amikacin, streptomycin, apramycin, or hygromycin (Table S2), although we cannot rule out that these antibiotics might induce *topAI* expression at concentrations other than those tested here. Indeed, a previous study showed that *topAI* RNA levels are strongly increased upon treatment with gentamicin (Kohanski et al., 2008). Another study showed that *topAI* levels are strongly induced upon treatment with kanamycin (Shaw et al., 2003), an antibiotic not tested in our work. In summary, *topAI* expression is modulated by a wide variety of mechanistically distinct ribosome-targeting antibiotics, reinforcing the idea that expression of this toxin-antitoxin system responds to the translation status of the cell.

To determine whether the relief of translation repression by ribosome-targeting antibiotics also prevents premature Rho-dependent transcription termination, we used ChIP-qPCR to measure the association of RNAP (β subunit) across the *topAI-yjhQP* operon in wild-type or *rho* mutant cells grown in the presence or absence of a sub-inhibitory concentration of tetracycline. As a control, we measured the association of RNAP within *rho*, where premature Rho-dependent transcription termination has been previously described (Bastet et al., 2017; Matsumoto et al., 1986). For analysis of RNAP association within *rho*, we normalized RNAP occupancy values to those in the *rhoL* region upstream; for *topAI-yjhQP*, we normalized RNAP occupancy values within the transcribed regions to those in the promoter region (Figure 3A). Mutation of *rho* led to a significant, 12.0-fold increase in RNAP occupancy within *rho* (t-test p = 0.001), consistent with Rho-dependent transcription termination early in the *rho* transcript (Figure 3B). Tetracycline treatment in wild-type cells did not lead to a significant increase in RNAP occupancy within *rho* (t-test p = 0.1). The combination of mutating *rho* and treating with tetracycline led to a significant, 5.9-fold increase in RNAP occupancy within *rho* (t-test p = 0.0009).

Mutation of *rho* led to significant, 3.6-, 18.9-, and 17.8-fold increases in RNAP occupancy at three positions across the *topAI-yjhQP* operon (Figure 3C; t-test p = 0.009, 0.004, 0.001, respectively). These data are consistent with Rho-dependent transcription termination within *topAI*. The larger increases in RNAP occupancy at later positions within the transcribed region are likely due to a combination of the limited spatial resolution of ChIP-qPCR, and the potential for multiple termination sites within the transcribed region. Tetracycline treatment in wild-type cells led to significant, 1.7-, 7.3-, and 6.7-fold increases in RNAP occupancy at the three positions across the *topAI-yjhQP* operon (t-test p = 0.03, 0.0009, 0.001, respectively), consistent with tetracycline treatment inhibiting Rho-dependent transcription termination within *topAI*. The combination of mutating *rho* and treating with tetracycline led to 2.0-, 5.7-, and 9.9-fold increases in RNAP occupancy at the three positions across the *topAI-yjhQP* operon (t-test p = 0.0004, 0.006, 0.005, respectively).

To determine whether the relief of translation repression by ribosome-targeting antibiotics affects the *topAI-yjhQP* RNA level, we used qRT-PCR to measure RNA levels at positions across the *topAI-yjhQP* operon in wild-type or *rho* mutant cells grown in the presence or absence of a sub-inhibitory concentration of tetracycline. Mutation of *rho* led to significant, 7.5-, 5-, and 8.4-fold increases in RNA levels at three positions across the *topAI-yjhQP* operon (Figure 3D; t-test p = 0.002, 0.002, $3.5e^{-7}$, respectively). These data are consistent with Rho-dependent transcription termination within *topAI*. Given that the most upstream region tested is upstream of the likely Rho termination site, these data suggest that premature Rho-dependent transcription termination destabilizes the *topAI-yjhQP* mRNA. Tetracycline treatment in wild-type cells led to significant, 4.9-, 2.0-, and 8.0-fold increases in RNA levels at the three positions across the *topAI-yjhQP* operon (t-test p = 0.008, 0.0007, $8.2e^{-6}$, respectively), consistent with tetracycline treatment inhibiting Rho-dependent transcription termination within *topAI*. The combination of mutating *rho* and treating with tetracycline led to 18.8-, 5.5-, and 19.9-fold increases in RNA levels at the three positions across the *topAI-yjhQP* operon (t-test p = 0.01, 0.006, 0.005, respectively). Together, our data support a model in which tetracycline treatment induces translation of *topAI*, which in turn prevents premature Rho-dependent transcription termination within *topAI*.

Expression of a uORF, *toiL*, is required for antibiotic-mediated *topAI* regulation

Long 5′ URs often contain regulatory elements such as uORFs that contribute to regulation of the downstream genes (Kriner et al., 2016). Given that *topAI* regulation responds to translation perturbation, we searched for a potential uORF that could act as a regulatory module in the *topAI* UR. Through manual inspection of available ribosome profiling data, we identified an 8-codon putative uORF that starts 139 nt upstream of *topAI* (Figure 4A) (Meydan et al., 2019; Wang et al., 2015; Weaver et al., 2019). A small protein (*Mia*-127) with near-identical amino acid sequence and relative genome position was described in *Salmonella enterica* (Figure 4, figure supplement 1) (Baek et al., 2017). To experimentally determine the frame and position of this uORF, which we renamed *toiL* (topoisomerase inhibitor leader) in *E. coli* K-12, we measured expression of a *toiL-lacZ* translational fusion. Replacing native codons with stop codons in the predicted CDS prevented expression of this fusion, unlike the equivalent substitution upstream of the ORF (Figure 4), supporting our ORF prediction.

The first 7 amino acids of the ToiL protein are conserved across bacteria that encode the *topAI-yjhQP* operon (Figure 4 – figure supplement 1).

To determine if *toiL* is a regulatory uORF, we tested whether expression of the *topAI-lux* translational reporter fusion is induced by ribosome-targeting antibiotics if *toiL* translation is impaired. We first mutated the start codon of *toiL* from 'ATG' to 'gTa' (Figure 5A; the specific substitutions were made to preserve the predicted secondary structure of the 5′ UR; Figure 5 – figure supplement 1A). The start codon mutation (Figure 5A; Figure 5 – figure supplement 1B) did not impact expression of a *topAI-lux* transcriptional reporter fusion that used the entire UR for *topAI* (Figure 5 – figure supplement 1C), indicating that the mutation does not cause premature Rho termination. We measured expression of the wild-type and mutant *topAI-lux* translational fusions in the presence or absence of sub-inhibitory concentrations of ribosome-targeting antibiotics. The *toiL* start codon mutation caused a 12- to 110-fold decrease in *topAI* induction by antibiotics (Figure 5B). Nonetheless, antibiotics were still able to modestly induce *topAI* expression. The *toiL* start codon is flanked by in-frame TTG and CTG trinucleotides that could potentially function as secondary start codons, perhaps explaining why mutation of the ATG start codon did not completely abolish the effect of antibiotic treatment. To test this possibility, we disrupted the predicted *toiL* Shine-Dalgarno (S-D) sequence (Figure 5A) and measured *topAI-lux* induction by ribosome-targeting antibiotics. Disruption of the *toiL* S-D site abolished induction of *topAI* expression by all antibiotics tested (Figure 5B), supporting the idea that active translation of *toiL* is absolutely required for *topAI* regulation by ribosome-targeting antibiotics.

Tetracycline causes de-repression of *topAI* translation by disrupting base-pairing around the *topAI* ribosome-binding site

Long URs that encode uORFs often utilize alternating RNA structures to modulate expression of the downstream gene (Kriner et al., 2016). For *topAI*, the class of regulatory element (i.e., a uORF) and the type of inducer (i.e., ribosome-targeting antibiotics) closely resembles the regulation of rRNA methyltransferase genes *ermB*/*ermC* (Subramanian et al., 2012), where stalling of the ribosome within a uORF in the presence of certain

macrolide antibiotics alters the downstream RNA structure, facilitating *ermB*/*ermC* translation. Computational prediction of the *topAI* UR RNA secondary structure suggests that sequences within *toiL* base-pair with the *topAI* ribosome-binding site (Figure 6A). Consistent with this prediction, the 5' UR of *toiL* has been reported to form an extended region of dsRNA (Lybecker et al., 2014). Base-pairing between *toiL* and the *topAI* ribosome-binding site is further supported by a structural prediction that incorporates sequence conservation information from orthologous regions in related species (Figure 6 – figure supplement 1).

We used in-cell SHAPE-seq (Watters et al., 2016a) to experimentally assess the *topAI* UR RNA secondary structure, and to investigate changes in secondary structure that occur upon tetracycline treatment. The SHAPE reagent, 1M7, penetrates live cells and modifies the backbone of accessible RNA nucleotides. In the subsequent RNA library preparation steps, modified nucleotides block reverse transcription (RT), creating RT-stop points that are detected bioinformatically after the 1M7-treated and untreated libraries are sequenced. Lower SHAPE reactivity is an indication of increased base-pairing interactions or nucleotide occlusion by other cellular factors such as ribosome binding. The SHAPE-seq data for untreated cells were in good agreement with the computationally predicted structure of the *topAI* UR (Figure 6A; Table S3): the beginning of the 5' mRNA end is highly reactive, as are predicted loops. We speculate that moderate reactivity in the *toiL* coding region is the result of translating ribosomes that temporarily disrupt the predicted long-range base-pairing interactions. Tetracycline treatment significantly altered reactivity ($p < 0.05$; see Methods for details) in two distinct regions in the 5′ region in comparison to the untreated control: sequence from the *toiL* S-D to the *toiL* start codon became less reactive, whereas the *topAI* S-D became more reactive (Figure 6B; Table S3). We propose that, in the presence of tetracycline, initiating ribosomes stall at the start of *toiL*, which leads to a decrease in base-pairing between *toiL* and the *topAI* S-D. No significant changes in the *toiL* ORF region were observed as a result of tetracycline treatment ($p > 0.05$), likely due to these nucleotides switching from occlusion by base-pairing to occlusion by a stalled ribosome. The increase in reactivity around the *topAI* S-D following tetracycline treatment is statistically significant, but modest, suggesting that loss of base-pairing between *toiL*

and this region is transient, and/or that a ribosome initiating translation of *topAI* partially prevents access to the SHAPE reagent.

Tetracycline stalls ribosomes at the start codon of *toiL* and at start codons across the transcriptome

To directly measure ribosome positioning within *toiL in vivo*, we used ribosome profiling to map ribosome occupancy across the *E. coli* transcriptome in untreated cells, and cells treated with tetracycline. A comparison of ribosome occupancy across all genes showed that *topAI* and its operonic genes *yjhQ* and *yjhP* are among the most strongly induced by tetracycline (Figure 7A; Table S4; note that induction could be at the level of RNA abundance, translation, or both). For cells treated with tetracycline, ribosome occupancy throughout *toiL* was substantially higher than in untreated cells. When mapping the 3' ends of ribosome-protected RNA fragments, we observed a strong peak at position +18 of *toiL*, a location consistent with the downstream edge of a ribosome stalled at the *toiL* start codon (Figure 7B). To determine whether tetracycline induces ribosome stalling in other ORFs, we compared ribosome occupancy in the region around the start codons of all annotated ORFs. Tetracycline induced stalling at positions +16 to +18 relative to start codons (Figure 7C), consistent with ribosomes stalled at start codons, as has been described for tetracycline in an earlier study (Nakahigashi et al., 2016). We conclude that tetracycline induces expression of *topAI* by stalling ribosomes at the start codon of *toiL*. We reasoned that retapamulin, a ribosome-targeting antibiotic that traps initiating ribosomes on start codons (Meydan et al., 2019; Yan et al., 2006) would induce *topAI* expression by the same mechanism. Consistent with this prediction, retapamulin strongly induced (~600-fold) expression of the *topAI-lux* translational reporter fusion (Figure 2C), and induction by retapamulin depended upon active translation of *toiL* (Figure 5B).

Mapping ribosome stalling sites induced by different antibiotics

At least five different ribosome-targeting antibiotics induce expression of *topAI-yjhQP* (Figure 2C). We speculated that these antibiotics, like tetracycline, induce *topAI-yjhQP* expression by stalling ribosomes within *toiL*, preventing base-pairing between the *toiL* ORF and the *topAI* S-D. Moreover, because these antibiotics have different targets within the ribosome and a range of mechanisms of action, we speculated that stalling

might occur at different positions in *toiL* depending on the antibiotic used. To further assess potential ribosome stalling at *toiL in vivo*, we used a modified version of a previously described stalling reporter construct (Bailey et al., 2008). Macrolide-mediated induction of this reporter relies on ribosome stalling at codon Ile9 of the *ermCL* uORF. We designed a hybrid construct where progressively longer segments of the *toiL* ORF, extending towards the 3' end, are fused to the *ermCL* 10th codon and the remaining downstream sequence, followed by a luciferase reporter gene (Figure 8A-B; Figure 8, figure supplement 1). These constructs include the RNA structural features from the *ermCL-ermC* intergenic region that are altered in response to ribosome stalling upstream. Thus, ribosome stalling within *toiL* sequences, close to the junction with *ermCL*, is expected to induce expression of the luciferase reporter gene (Figure 8A; Figure 8 – figure supplement 1). We measured expression of the stalling reporter constructs in a strain lacking *topAI* and *yjhQ*. As a control, we replaced *toiL* with the native *ermCL* sequence to show that this reporter is responsive to erythromycin treatment, but not other antibiotics (Figure 8 – figure supplement 2). Tetracycline and retapamulin induced expression most strongly with the fusion to the start codon of *toiL* (Figure 8C), consistent with ribosome stalling at the start codon. Tylosin induced expression of only the 5-codon fusion reporter construct, suggesting tylosin-induced stalling at Val5. The effect of tylosin on expression of this reporter was abolished by the Val5→Leu mutation (Figure 8C). Interestingly, tetracycline, retapamulin and erythromycin also showed some induction with the 5-codon *toiL* fusion, with the effect reduced by the Val5→Leu mutation (Figure 8C); additional stalling at this codon might have an additive effect on *topAI* induction. Erythromycin induced expression most strongly with the construct that has the complete *toiL* ORF, including the stop codon (Figure 8C), suggesting that ribosomes stall during translation termination. Spectinomycin induced expression of several constructs, but the level of induction was lower than for other antibiotics (Figure 8C), despite being able to induce *topAI* to a similar extent to tetracycline (Figure 2C). Chloramphenicol did not induce expression of any of the constructs, consistent with its inability to induce expression of *topAI* (Figure 2C). Overall, these data suggest that a variety of ribosome-targeting antibiotics cause ribosomes to stall within *toiL*, with different antibiotics stalling ribosomes at different positions. Moreover, the data suggest that ribosome stalling at a variety of positions within *toiL* is sufficient to induce *topAI-yjhQP* expression.

DISCUSSION

Model for *topAI* regulation

We propose the following model for *topAI* regulation (Figure 9): In the absence of translation stress, a hairpin that encompasses the *toiL* uORF and the *topAI* ribosome-binding side prevents initiation of *topAI* translation, which in turn promotes premature Rho-dependent transcription termination within the *topAI* ORF. Under these repressive conditions, *toiL* is presumably being efficiently translated, but ribosomes translating *toiL* only transiently disrupt the hairpin. Upon induction of certain types of translation stress, notably ribosome inhibition by select antibiotics, ribosomes stall within *toiL*, disrupting the repressive hairpin and leading to translation of *topAI*, which in turn prevents Rho-dependent transcription termination within *topAI*. *topAI-yjhQP* RNA levels in the *rho* R66S mutant increase ~2-fold upon tetracycline treatment (Figure 3D), suggesting an additional, albeit modest level of regulation at the level of mRNA stability. This could be due to a stabilizing effect of translation (Deana and Belasco, 2005), or direct regulation of RNase accessibility in the 5' UR.

toiL is a multipurpose sensory uORF

Sensory uORFs are versatile regulators that have evolved to rapidly alter physiology in response to a wide variety of environmental stresses that impact translation. However, most regulatory uORFs characterized to date have been proposed to respond to a single translational stress. By contrast, *toiL* senses a wide variety of ribosome-targeting antibiotics with unrelated mechanisms of action. The ability of *toiL* to transduce a wide range of translational stress signals is likely due to the fact that base-pairing with the *topAI* ribosome-binding site occurs across the length of the *toiL* ORF; hence, ribosome stalling anywhere within *toiL* would likely prevent hairpin formation, relieving *topAI* repression. This likely explains why mutations in helix 69 and helix 80 of the 23S rRNA induce expression of *topAI*, since residues in these helices have been reported to promote ribosome processivity (Kipper et al., 2009; Samaha et al., 1995), and the impact of ribosomes slowing as they translate *toiL* could be similar to that of a ribosome stall. Many antibiotics have been shown to stall ribosomes in ORFs in a sequence-specific manner (Orelle et al., 2013; Vázquez-Laslop and Mankin, 2018a). We speculate

that the *toiL* sequence has evolved to stall ribosomes in a sequence-specific manner in response to a variety of antibiotics.

There are a few other examples of uORFs where more than one class of antibiotic can induce ribosome stalling. *Clostridiodes difficile cplR* is regulated by a uORF that senses retapamulin and lincomycin (Obana et al., 2023). *Bacillus subtilis vmlR* is regulated by a uORF that senses retapamulin, lincomycin, iboxamycin (Takada et al., 2022). And *Staphylococcus haemolyticus vga(A)* is regulated by a uORF that senses lincosamides, streptogramin A, and pleuromutilins (Vimberg et al., 2020). However, in these cases, the antibiotics all likely function to stall ribosomes at start codons (Takada et al., 2022). Hence, even though the antibiotics have different targets within the ribosome, the position of ribosome stalling is the likely to be the same. By contrast, our data strongly suggest that while tetracycline and retapamulin stall ribosomes at the *toiL* start codon, tylosin, spectinomycin and erythromycin stall ribosomes further downstream.

Another uORF that is known to sense multiple classes of ribosome-targeting antibiotics is found upstream of the actinobacterial gene *whiB7* (Burian and Thompson, 2018; Lee et al., 2022). Whether antibiotics induce ribosome stalling within the *whiB7*-associated uORF has not been tested. Intriguingly, *whiB7* expression can also be induced by amino acid starvation (Lee et al., 2022), suggesting that non-antibiotic stresses that lead to ribosome stalling within the uORF can also contribute to regulation. An artificial uORF-regulated reporter construct has also been generated that responds to a variety of ribosome-targeting antibiotics, albeit to lesser extent than *topAI* or *whiB7*; the mechanism of uORF regulation in response to antibiotic treatment was presumed to involve ribosome stalling in the uORF, although this has not been tested (Osterman et al., 2012).

Understanding how different antibiotics stall ribosomes within *toiL*

The mechanism by which tetracycline stalls ribosomes at start codons has not been determined. Tetracycline binds to the 30S ribosomal subunit in the decoding center, and likely functions by preventing association of aminoacyl-tRNAs with the A-site (Nguyen et al., 2014). We speculate that tetracycline binds to initiating

ribosomes when the A-site is free, preventing association of an aminoacyl-tRNA in the A-site, an essential step prior to formation of the first peptide bond in the nascent peptide. Intriguingly, regulation of tetracycline resistance can involve a uORF (Chopra and Roberts, 2001), including one case where the uORF is only four codons long (Wang et al., 2005), consistent with regulation by ribosome stalling at the start codon.

Macrolides such as erythromycin function by binding in the nascent peptide exit tunnel of the ribosome (Vázquez-Laslop and Mankin, 2018b). Ribosome stalling induced by erythromycin is well-established for uORFs upstream of macrolide-resistance genes (Ramu et al., 2009), where the nascent peptide in the exit tunnel senses the presence of erythromycin, leading to structural changes that prevent peptide bond formation. Our data are consistent with erythromycin inducing ribosome stalling at the end of *toiL* (Figure 8C), suggesting that the nascent peptide senses erythromycin, leading to structural changes that inhibit the action of release factors. Indeed, erythromycin was recently shown to stall ribosomes at the penultimate codon of the *Streptococcus msrDL* uORF by altering the 23S rRNA structure to prevent release factor binding (Fostier et al., 2023). When ribosomes stall on *msrDL* in the presence of erythromycin, the N_{-3} and N_{-2} amino acids with respect to the C-terminal residue are leucine and isoleucine respectively, and the stop codon is UAA. The N_{-3} and N_{-2} amino acids are the closest to erythromycin in the peptide exit tunnel (Fostier et al., 2023). Assuming erythromycin induces stalling of ribosomes on the penultimate codon of *toiL*, the N_{-3} and N_{-2} amino acids amino acids would be valine and isoleucine, respectively, and the stop codon is UAA, suggesting a similar interaction of the ToiL and MsrDL nascent peptides with erythromycin, and a similar mechanism of stalling.

Tylosin is also a macrolide, and stalling induced by tylosin has also been observed previously at an RYR sequence in *Bacillus subtilis* (Yakhnin et al., 2019). This suggests a similar mechanism of action to erythromycin, which can stall ribosomes at R/K-X-R/K motifs (Davis et al., 2014; Ramu et al., 2009). By contrast, our data suggest that tylosin induces ribosome stalling at Val5 of *toiL* (Figure 8C). Despite the apparent preference for R/K-X-R/K motifs for tylosin-induced ribosome stalling, tylosin has been observed to

stall ribosomes at other sequences (Orelle et al., 2013), suggesting that the sequence requirements for tylosin-induced stalling are complex, as they are for erythromycin (Ramu et al., 2009).

Spectinomycin also induces expression of *topAI* in a *toiL*-dependent manner, although our data suggest that spectinomycin does not lead to ribosome stalling at a single codon position in *toiL* (Figure 8C). Little is known about the effects of spectinomycin on ribosome stalling, but it has been shown to stall ribosomes at specific sequences within ORFs (Orelle et al., 2013).

We did not observe any induction of *topAI* expression by chloramphenicol. Previous studies have shown that chloramphenicol stalls ribosomes in a sequence-specific manner, with stalling most pronounced immediately following an alanine, serine or threonine codon (Marks et al., 2016; Syroegin et al., 2022). The lack of alanine, serine and threonine codons in *toiL* may explain the apparent lack of stalling induced by chloramphenicol.

The link between translation attenuation and premature Rho-dependent termination

In addition to directly regulating translation of *topAI*, *toiL* indirectly regulates *topAI* transcription by modulating Rho-dependent transcription termination within the *topAI* ORF. We speculate that Rho prematurely terminates transcription of other uORF-regulated genes where the uORF modulates translation, similar to the function of some riboswitches (Bastet et al., 2018). Other studies of premature Rho termination events within coding regions suggested that termination occurs due to the unmasking of Ruts within the ORF that are otherwise occluded by translating ribosomes (Bastet et al., 2017; Ben-Zvi et al., 2019; Bossi et al., 2012; de Smit et al., 2008). By contrast, the Rut for *topAI* is located within the 5′ UR. This suggests that the mechanism by which translation of *topAI* prevents Rho termination is distinct to that of other characterized examples of prematurely Rho-terminated genes. Specifically, ribosomes translating *topAI* likely prevent Rho from catching the elongating RNAP, rather than preventing Rho loading onto the nascent RNA. If there are indeed two distinct mechanisms by which ribosomes can prevent Rho termination, the level of translation required for each

mechanism may be different. An alternative possibility is that the *topAI* Rut is very long and extends into the *topAI* ORF, in which case ribosomes could prevent Rho termination by preventing Rho loading.

We identified elements of the *topAI* Rut that are located a short distance upstream of *toiL*. Given the length of RNA required to constitute a Rut, the *topAI* Rut must overlap *toiL*. Thus, the Rut is functional despite the presence of an overlapping ORF that is actively translated. We propose that (i) Rho can only load onto the *topAI* 5′ region after translation of *toiL* is terminated, or (ii) Rho can loop the RNA around the *toiL* region to access upstream and downstream elements of the Rut. It has previously been proposed that Rho can step over an RNA roadblock to access available Ruts (Kriner and Groisman, 2017; Schwartz et al., 2007), thereby helping Rho to overcome roadblocks in the 5′ region.

Concluding remarks

uORFs permit rapid regulation in response to translational stress. For almost all previous uORFs shown to sense antibiotics, the downstream gene is functionally related to antibiotic resistance, often directly promoting resistance to the antibiotic(s) that induce expression. Although *topAI* has been characterized as a DNA gyrase inhibitor (Yamaguchi and Inouye, 2015), we speculate that *topAI* and/or *yjhQ*/*P*, which are transcribed from the same operon, have additional functions that are linked to the small molecule that *toiL* has evolved to sense. This small molecule could be a ribosome-targeting antibiotic, or a non-antibiotic molecule such as an amino acid or polyamine, which promote ribosome stalling in other uORFs (Herrero Del Valle et al., 2020; van der Stel et al., 2021).

There has been a recent explosion in the discovery of bacterial sORFs, many of which are located short distances upstream of canonical ORFs on the same strand (Meydan et al., 2019; Smith et al., 2022; Stringer et al., 2021; Venturini et al., 2020; Weaver et al., 2019). We speculate that there are large numbers of regulatory uORFs even in a well-characterized bacterium like *E. coli*. Indeed, analysis of ribosome profiling data for cells

treated with tetracycline revealed >5-fold increases in ribosome-associated RNA levels relative to untreated cells for several genes that are known to be associated with a uORF (Table S4), including *mgtA*, *corA* and *speC*.

MATERIALS AND METHODS

Strains and plasmids

All strains and plasmids used in this study are listed in Table S5. All oligonucleotides used in this study are listed in Table S6. An *E. coli* MG1655 Δ*lacZ* Δ*topAI-yjhQ*::*thyA* strain (GB001) was constructed using the FRUIT recombineering method (Stringer et al., 2012). Briefly, the *thyA* gene was amplified using primers JW7676 + JW7677 and electroporated into strain AMD189 (MG1655 Δ*lacZ* Δ*thyA*) (Stringer et al., 2012) to replace the *topAI* gene from 379 bp upstream of *topAI* to 74 bp into the *yjhQ* coding region.

All *topAI* and *toiL lacZ* and luciferase reporter plasmids (pJTW100, pGB164, pGB182, pGB196, pGB197, pGB200, pGB201, pGB202, pGB215, pGB217, pGB297, pGB305, pGB306, pGB313) were made to include sequence starting at -400 bp upstream of *topAI* and were presumed to include the native *topAI* promoter. Fusions to *lacZ* are derivatives plasmid pAMD033 (Dornenburg et al., 2010). Fusions to luciferase are derivatives of pGB135, which includes the *luxCDABE* operon from *Photorhabdus luminescens*. Constructing pGB135 first required construction of plasmid pGB96. pGB96 was made by PCR-amplification of a region from plasmid pJTW064 (Stringer et al., 2014) using primers JW8044 + JW8045, PCR-amplification of a region from pCS-PesaRlux (Shong and Collins, 2013) using primers JW8046 + JW8047, combining the two PCR products using splicing by overlap extension (Horton et al., 1990), and cloning the resultant product into pET-PesaRlux cut with *Xho*I and *Xba*I (Shong and Collins, 2013). pGB135 was made by PCR-amplification of two regions from pGB96 using primers JW8044 + JW8522 and JW8523 + JW8047, combining the two PCR products using splicing by overlap extension (Horton et al., 1990), and cloning the resultant product into pCS-PesaRlux cut with *Xho*I and *Xba*I (Shong and Collins, 2013). pGB135 has the P*esaR* fragment from pCS-PesaRlux replaced with a constitutive promoter and convenient restriction sites for transcriptional or translation fusions to the *luxC* gene; transcriptional reporter fusions included a Shine-Dalgarno sequence, whereas translational fusions used the sequence up to the initiation codon of the gene of interest followed by the second codon of the reporter gene.

Plasmid pJTW100 is a derivative of pAMD033 that includes a full-length *topAI* gene and the first 90 bp of *yjhQ* translationally fused to *lacZ*. pJTW100 was constructed by PCR-amplifying from an *E. coli* MG1655 colony using primers JW5638 + JW5639, and cloning the resultant PCR product into pAMD033 (Dornenburg et al., 2010) cut with *Sph*I and *Hin*dIII.

Plasmids pGB215 and pGB217 are derivatives of pAMD033 with sequence up to position +10 or +42 of *topAI* (relative to the start codon) fused transcriptionally to *lacZ*. pGB215 and pGB217 were made by PCR-amplification from an *E. coli* MG1655 colony using primers JW5638 + JW9453 or JW5638 + JW9154, respectively, and cloning of the result PCR products into the *Sph*I and *Nhe*I sites of pAMD033 (Dornenburg et al., 2010). Plasmids pGB305 and pGB306 are equivalent to plasmids pGB215 and pGB217, except that they have a mutated *rut* in the 5′ UR (4C → 4A). They were constructed identically to pGB215 and pGB217 except that the PCRs used primers JW5638 + JW9453/JW9154, and the template for the PCR was plasmid pGB299. Plasmid pGB299 is a derivative of pAMD033 (Dornenburg et al., 2010) with the complete *topAI* gene (not including the stop codon) fused translationally to *lacZ*, with a mutated *rut* in the 5′ UR (4C → 4A). pGB299 was constructed by PCR-amplifying from an *E. coli* MG1655 colony using primers JW5638 + JW9803 and JW9804 + JW8023, combining the two PCR products using splicing by overlap extension (Horton et al., 1990), and cloning the resultant product into pAMD033 cut with *Sph*I and *Hin*dIII.

Plasmid pGB214 is equivalent to pJTW100 except that it has a mutation in the *toiL* start codon (ATG→gTa). pGB214 was constructed by PCR-amplifying from an *E. coli* MG1655 colony using primers JW5638 + JW9139 and JW9138 + JW5639, combining the two PCR products using splicing by overlap extension (Horton et al., 1990), and cloning the resultant PCR product into pAMD033 (Dornenburg et al., 2010) cut with *Sph*I and *Hin*dIII. Plasmids pGB182 (wild-type) and pGB297 (*toiL* ATG→gTa) include the complete *topAI* 5′ UR transcriptionally fused to *lacZ*. pGB182 and pGB297 were made by PCR-amplifying from an *E. coli* MG1655

colony or pGB214, respectively, using primers JW5638 + JW8809, and cloning the resultant PCR product into pAMD033 (Dornenburg et al., 2010) cut with *Sph*I and *Nhe*I.

Plasmid pGB164 is a derivative of pAMD033 with the full *toiL* gene (not including the stop codon) fused translationally to *lacZ*. Plasmids pGB196 (AAT→tga), pGB197 (CTG→tga), pGB200 (ATG→tga), and pGB201 (TTG→tga) are mutant derivatives of pGB164. pGB164 was made by PCR-amplifying from an *E. coli* MG1655 colony using primers JW5638 + JW8741, and cloning the resultant PCR product into pAMD033 (Dornenburg et al., 2010) cut with *Sph*I and *Hin*dIII. pGB196, pGB197, pGB200, and pGB201 were cloned identically except that primer JW8741 was replaced with JW8999, JW8998, JW9013, and JW9014, respectively.

Plasmid pGB202 is a derivative of pGB135 with a translational fusion of the *topAI* start codon to luciferase. pGB313 is a derivative of pGB202 with a *toiL* start codon mutation. pGB202 and pGB313 were made by PCR-amplifying from an *E. coli* MG1655 colony or pGB214, respectively, using primers JW9288 + JW9289, and cloning the resultant PCR product into pGB135 cut with *Bam*HI and *Eco*RI. Plasmid pGB366 is a derivative of pGB202 with a *toiL* Shine-Dalgarno sequence mutation. pGB366 was made by PCR-amplifying from an *E. coli* MG1655 colony using primers JW9288 + JW10873 and JW10874 + JW9289, combining the two PCR products using splicing by overlap extension (Horton et al., 1990), and cloning the resultant product into pGB135 cut with *Bam*HI and *Eco*RI.

Plasmids pGB323, pGB324, pGB325, pGB326, pGB327, pGB328, pGB329, pGB346, and pGB347 include sequences that extend to different positions within *toiL* fused translationally to the *ermCL* gene from the 10th codon, which is fused translationally to luciferase. pGB323, pGB324, pGB325, pGB326, pGB327, pGB328, pGB329, pGB346, and pGB347 were made by PCR-amplifying (i) from an *E. coli* MG1655 colony using primer JW9288 and each of JW9989, JW10122, JW10144, JW10145, JW10146, JW10147, JW10148, JW101848, and JW10849, respectively, and (ii) from geneBlock GB007 (Supplementary Table 6) using primers JW10123 + JW9965. Pairs of PCR products were combined using splicing by overlap extension (Horton et al.,

1990), and the resultant products were cloned into pGB135 cut with *Bam*HI and *Eco*RI. pGB308 is equivalent to these plasmids except *toiL* coding sequence was replaced with the beginning of the *ermCL* sequence (codons 1-9). pGB308 was made by PCR-amplifying (i) from an *E. coli* MG1655 colony using primer JW9288 + JW9989, and (ii) from geneBlock GB007 (Table S6) using primers JW9990 + JW9965. Pairs of PCR products were combined using splicing by overlap extension (Horton et al., 1990), and the resultant products were cloned into pGB135 cut with *Bam*HI and *Eco*RI.

Plasmids pGB322 and pGB318 are derivatives of pPro24 (Lee and Keasling, 2005), which contains a propionate-inducible promoter. pGB322 and pGB318 include a complete rRNA operon, either wild-type or mutant (ΔT1917 23S rRNA), respectively. The rRNA operons in both plasmids are fusions of the *rrnB* (upstream of 23S position +1917) and *rrnC* (position +1917 and downstream) operons. pGB318 was made first by PCR-amplifying from an *E. coli* MG1655 colony using primers JW10036 + JW9737 and JW9740 + JW10037, combining the two PCR products using splicing by overlap extension (Horton et al., 1990), and cloning the resultant product into pPro24 cut with *Nhe*I and *Bam*HI. pGB322 was made by PCR-amplifying from pGB318 using primers JW10036 + JW10104 and JW9740 + JW10105, combining the two PCR products using splicing by overlap extension (Horton et al., 1990), and cloning the resultant product into pPro24 cut with *Nhe*I and *Bam*HI.

Plasmid pGB72 is a derivative of pET-PesaRlux (Shong and Collins, 2013) that has a constitutive promoter (Burr et al., 2000) followed by 568 bp of a reverse-complemented *Hin*dIII fragment from the *rrsB* gene that is known to function as a Rho terminator (Li et al., 1984). pGB72 was made by annealing and extending primers JW7977b+7979b, PCR-amplifying from plasmid pSL103 (Li et al., 1984) using primers JW7994 and J7995, combining the two PCR products using splicing by overlap extension (Horton et al., 1990), and cloning the resultant product into pET-PesaRlux cut with *Xho*I and *Bam*HI.

Isolation and identification of *trans*-acting mutants

The trans-acting mutant genetic selection was performed as described previously (Baniulyte et al., 2017). Briefly, cultures of MG1655 Δ*lacZ* with pJTW100 were grown at 37 °C in LB medium. 100 µl of overnight culture was washed and plated on M9 + 0.2% lactose agar. Spontaneous survivors were tested for increased plasmid copy number or *cis*-acting mutations near *topAI*; these mutants were eliminated. Chromosomal mutations were identified either by PCR-amplification and sequencing of *rho* or by whole-genome sequencing. Mutants identified this way included F62S, F62V, G63V (isolated three times), R66C, R66S, Y80C, Y80D, Y80N, Y80S, S82F (isolated twice), and P138L. Rho mutants were also detected by transducing a wild-type *rho* locus and looking for phenotypic reversion, or by introducing and assaying a Rho-dependent termination luciferase reporter plasmid (pGB72). Total genomic DNA was extracted from the three remaining mutants following the manufacturer's protocol (Qiagen, catalog # 69504). SNPs were identified using whole-genome sequencing, as described previously (Singh et al., 2016).

Quantification of RNAP association with DNA by chromatin immunoprecipitation coupled with real-time PCR (ChIP-qPCR)

20 ml *E. coli* wild-type (MG1655) or *rho* mutant (CRB016) cells were grown in LB at 37 °C with shaking. When the cultures reached an OD_{600} of ~1.0, tetracycline (Sigma #T3383) was added to one set of samples at a final concentration of 0.5 µg/ml. All untreated and tetracycline-treated samples (three biological replicates) were left at 37 °C with shaking for 17 min, after which 500 µl of each sample was pelleted and frozen for total RNA extraction later. For ChIP, the remainder of each sample was crosslinked with 1% formaldehyde (final concentration), and processed as previously described (Stringer et al., 2014). For immunoprecipitation, 800 µl of crosslinked chromatin was incubated with 25 µl Protein A Sepharose slurry (50%) in TBS and 1 µl of antibody against RNAP β (Biolegend, #663003, clone: NT63) for 90 minutes at room temperature while rotating. RNAP enrichment was normalized using the $2^{-\Delta\Delta Ct}$ method to the corresponding "input" control sample and either the *rhoL* region (for measurements within *rho*) or the *topAI* promoter region (for measurements within *topAI-yjhQP*), as previously described (Bastet et al., 2017). All real-time PCR samples were set up in technical duplicates.

Quantification of RNA levels by reverse transcription coupled with real-time PCR (RT-qPCR)

Total RNA was extracted from frozen pellets (see above) using a Quick-RNA Miniprep Kit (Zymo Research, #R1054) following the manufacturer's protocol. Approximately 136 ng of total RNA for each sample was reverse-transcribed using MultiScribe Reverse Transcriptase (Invitrogen, #4311235) following the manufacturer's protocol. A "no reverse transcriptase" control was also included to assess DNA contamination. The resulting cDNA was diluted 1:3 and used as a template for quantitative real-time PCR. RNA expression values were obtained using the $2^{-\Delta\Delta Ct}$ method, normalizing to a region within the *mreB* gene. Values were further normalized to those in wild-type cells (MG1655) without tetracycline treatment. All real-time PCR samples were set up in technical duplicates.

RNA structural prediction using sequence identity among homologues

We used PETfold (Seemann et al., 2011, 2008) to predict the *topAI* UR RNA secondary structure based on a sequence alignment of selected homologous sequences (Figure 6 – figure supplement 1A). All sequences are from species with at least 50% TopAI amino acid identity to the *E. coli* K-12 protein.

SHAPE-seq

A total of three biological replicates of the strain GB001 + pJTW100 were grown to an OD_{600} of ~1.2 in LB medium at 37 °C. Cultures were split, and one set of two replicates was treated with 0.2 μg/ml tetracycline (T3383, Sigma) for 90 min. Cultures were subjected to the in-cell SHAPE-seq procedure previously described for poorly expressed mRNAs (Watters et al., 2016a). The SHAPE reagent 1M7 was purchased from MedChem Express (HY-D0913). SHAPE-seq libraries were sequenced using an Illumina MiSeq instrument (251 nt, paired-end reads). Sequencing data were analyzed using the *spats* pipeline (Watters et al., 2016a, 2016b). Raw reactivities are listed in Table S3. Significant changes in reactivity and corresponding adjusted *p*-values upon tetracycline treatment were determined using the DESeq2 R package (Love et al., 2014), comparing untreated

and tetracycline treated sample reactivities at each position using three ("Untreated") and two ("Treated") biological replicates from each sample. The mRNA structure of the *topAI* UR (Figure 6A) was predicted using mFOLD (Zuker, 2003) and drawn using StructureEditor (https://rna.urmc.rochester.edu/GUI/html/StructureEditor.html).

Reporter assays

Bacterial cultures for luciferase or β-galactosidase assays were grown at 37 °C in LB medium to an OD_{600} of 0.5–0.6 unless otherwise indicated in the figure legend. Cultures were grown in 15 ml round-bottom tubes except for antibiotic titration assays (Table S2; see below). Tetracycline (Sigma #T3383), spectinomycin (Sigma-Aldrich #S4014), erythromycin (Sigma-Aldrich #E5389), retapamulin (Sigma-Aldrich #CDS023386), tylosin (Sigma-Aldrich #T6134), chloramphenicol (Sigma-Aldrich #C0378), kasugamycin, gentamicin (Sigma-Aldrich #G1272), amikacin, streptomycin, apramycin, or hygromycin (Millipore #400052) antibiotics were added at indicated concentrations and timepoints. Reported epidemiological cut-off values for antibiotics reported by EUCAST (Kahlmeter and Turnidge, 2022) are: tetracycline, 8 μg/ml; spectinomycin, 64 μg/ml; chloramphenicol, 16 μg/ml; gentamicin, 2 μg/ml; amikacin, 8 μg/ml; streptomycin, 16 μg/ml. Minimum inhibitory concentrations (MICs) have been reported for tylosin, 512 μg/ml (Andersen et al., 2012); kasugamycin, 500 μg/ml (Lange et al., 2017); erythromycin, 150 μg/ml (Suvorov et al., 1988); apramycin, 32 μg/ml (Yang et al., 2020); retapamulin, 12.5 μg/ml (Meydan et al., 2019); and hygromycin, 150 μg/ml (McGaha and Champney, 2007). These values were used as a guide for selecting antibiotic concentrations to test in reporter assays. MICs can vary considerably between strains, so the MICs and epidemiological cut-off values listed above may differ from the actual values for *E. coli* K-12.

Plasmid-encoded wild-type and mutant rRNA overexpression (Figure 2B) was induced by adding 12 mM sodium propionate (Sigma-Aldrich #P1880) to bacterial cultures at an OD_{600} of ~0.2. β-galactosidase assays were performed as previously described (Baniulyte et al., 2017). For luciferase assays, each cell culture (200 μl) was aliquoted into a 96-well plate with four technical replicates each. Luminescence readings for were taken

using a Biotek Synergy 2 instrument. Luminescence counts (RLU) were adjusted for OD_{600} and reported as RLU/OD_{600}. Antibiotic concentrations and lengths of treatments are indicated in the figure legends. Antibiotic titration assays (Table S2) were performed in 96-well deep-well plates. Briefly, 1.5 ml of GB001 cells containing the pGB202 plasmid was grown to an OD_{600} of ~1.0, aliquoted into a 96-well deep-well plate, and treated with antibiotics at the indicated concentrations for 90 min. 100 μL of each bacterial culture was used for luminescence detection, as described above.

Ribosome profiling (Ribo-seq)

200 ml of *E. coli* MG1655 cells were grown in LB ± 1 μg/ml tetracycline to an OD_{600} of ~1.1. Filtering was started at 17 min post-treatment. Monosomes were isolated and libraries were constructed as previously described (Smith et al., 2022), with minor modifications: the 3'-linked oligonucleotide ligation reaction was carried out overnight at 16 °C; circularized, reverse-transcribed cDNA was PCR-amplified for 6-8 cycles using universal primer JW8835 and sample-specific primers JW3249 (no antibiotic) or JW10755 (tetracycline).

Determination of Ribo-seq sequence read coverage was performed as described previously (Smith et al., 2022). Briefly, sequence reads were trimmed using a custom Python script to remove the ligated adaptor sequence, and mapped to reference genome MG1655 NC_000913.3 using Rockhopper (McClure et al., 2013). Sequence read coverage for sequence 3' ends (presumed to correspond to the positions of the downstream edge of ribosomes) was determined for the whole genome, normalizing to total read count (reads per million; RPM). The metagene plot showing sequence read coverage around start codons (Figure 7C) was generated as described previously (Smith et al., 2022). Normalized Ribo-seq coverage for all annotated ORFs was determined using differential expression analysis with Rockhopper (McClure et al., 2013), excluding the first and last 30 nt of each gene.

ACKNOWLEDGEMENTS

We thank Randall Morse, Pan Li, and Allen Buskirk for helpful comments on the manuscript. We thank the Wadsworth Center Applied Genomic Technologies Core Facility for DNA sequencing. We thank the Wadsworth Center Tissue Culture and Media Core Facility and Glassware Facility for technical support.

FUNDING INFORMATION

This work was supported in part by the NIH Director's New Innovator Award Program, 1DP2OD007188 (J.T.W.) and National Institutes of Health grant 1R35GM144328 (J.T.W.).

DATA AVAILABILITY

Raw Illumina sequencing data are available from EBI ArrayExpress using accession numbers E-MTAB-8365 (SHAPE-seq) and E-MTAB-12242 (Ribo-seq).

REFERENCES

Adams PP, Baniulyte G, Esnault C, Chegireddy K, Singh N, Monge M, Dale RK, Storz G, Wade JT. 2021. Regulatory roles of Escherichia coli 5' UTR and ORF-internal RNAs detected by 3' end mapping. *Elife* **10**:e62438. doi:10.7554/eLife.62438

Adhya S, Gottesman M. 1978. Control of Transcription Termination. *Annual Review of Biochemistry* **47**:967–996. doi:10.1146/annurev.bi.47.070178.004535

Alifano P, Rivellini F, Limauro D, Bruni CB, Carlomagno MS. 1991. A consensus motif common to all rho-dependent prokaryotic transcription terminators. *Cell* **64**:553–563. doi:10.1016/0092-8674(91)90239-U

Andersen NM, Poehlsgaard J, Warrass R, Douthwaite S. 2012. Inhibition of protein synthesis on the ribosome by tildipirosin compared with other veterinary macrolides. *Antimicrob Agents Chemother* **56**:6033–6036. doi:10.1128/AAC.01250-12

Baek J, Lee J, Yoon K, Lee H. 2017. Identification of Unannotated Small Genes in Salmonella. *G3: Genes, Genomes, Genetics* **7**:983–989. doi:10.1534/g3.116.036939

Bailey M, Chettiath T, Mankin AS. 2008. Induction of erm(C) expression by noninducing antibiotics. *Antimicrobial Agents and Chemotherapy* **52**:866–874. doi:10.1128/AAC.01266-07

Baniulyte G, Singh N, Benoit C, Johnson R, Ferguson R, Paramo M, Stringer AM, Scott A, Lapierre P, Wade JT. 2017. Identification of regulatory targets for the bacterial Nus factor complex. *Nature Communications* **8**:2027. doi:10.1038/s41467-017-02124-9

Bastet L, Chauvier A, Singh N, Lussier A, Lamontagne A-M, Prévost K, Massé E, Wade JT, Lafontaine DA. 2017. Translational control and Rho-dependent transcription termination are intimately linked in riboswitch regulation. *Nucleic Acids Research* **45**:7474–7486. doi:10.1093/nar/gkx434

Bastet L, Turcotte P, Wade JT, Lafontaine DA. 2018. Maestro of regulation: Riboswitches orchestrate gene expression at the levels of translation, transcription and mRNA decay. *RNA Biol* **15**:679–682. doi:10.1080/15476286.2018.1451721

Ben-Zvi T, Pushkarev A, Seri H, Elgrably-Weiss M, Papenfort K, Altuvia S. 2019. mRNA dynamics and alternative conformations adopted under low and high arginine concentrations control polyamine biosynthesis in Salmonella. *PLoS Genetics* **15**:e1007646. doi:10.1371/journal.pgen.1007646

Bernhart SH, Hofacker IL, Will S, Gruber AR, Stadler PF. 2008. RNAalifold: improved consensus structure prediction for RNA alignments. *BMC Bioinformatics* **9**:474. doi:10.1186/1471-2105-9-474

Bossi L, Schwartz A, Guillemardet B, Boudvillain M, Figueroa-Bossi N. 2012. A role for Rho-dependent polarity in gene regulation by a noncoding small RNA. *Genes and Development* **26**:1864–73. doi:10.1101/gad.195412.112

Breaker RR. 2018. Riboswitches and Translation Control. *Cold Spring Harbor perspectives in biology* **10**:a032797. doi:10.1101/cshperspect.a032797

Burian J, Thompson CJ. 2018. Regulatory genes coordinating antibiotic-induced changes in promoter activity and early transcriptional termination of the mycobacterial intrinsic resistance gene whiB7. *Mol Microbiol* **107**:402–415. doi:10.1111/mmi.13890

Burmann BM, Schweimer K, Luo X, Wahl MC, Stitt BL, Gottesman ME, Rosch P. 2010. A NusE:NusG Complex Links Transcription and Translation. *Science* **328**:501–504. doi:10.1126/science.1184953

Burr T, Mitchell J, Kolb A, Minchin S, Busby S. 2000. DNA sequence elements located immediately upstream of the -10 hexamer in Escherichia coli promoters: a systematic study. *Nucleic acids research* **28**:1864–70.

Cardinale CJ, Washburn RS, Tadigotla VR, Brown LM, Gottesman ME, Nudler E. 2008. Termination factor Rho and its cofactors NusA and NusG silence foreign DNA in E. coli. *Science (New York, NY)* **320**:935–8. doi:10.1126/science.1152763

Chhakchhuak PIR, Khatri A, Sen R. 2018. Mechanism of Action of Bacterial Transcription Terminator Rho. *Proceedings of the Indian National Science Academy*. doi:10.16943/ptinsa/2018/49436

Chopra I, Roberts M. 2001. Tetracycline Antibiotics: Mode of Action, Applications, Molecular Biology, and Epidemiology of Bacterial Resistance. *Microbiology and Molecular Biology Reviews*. doi:10.1128/mmbr.65.2.232-260.2001

Dar D, Sorek R. 2018. High-resolution RNA 3-ends mapping of bacterial Rho-dependent transcripts. *Nucleic Acids Research*. doi:10.1093/nar/gky274

Davis AR, Gohara DW, Yap M-NF. 2014. Sequence selectivity of macrolide-induced translational attenuation. *Proceedings of the National Academy of Sciences* **111**:15379–15384. doi:10.1073/pnas.1410356111

de Smit MH, Verlaan PWG, van Duin J, Pleij CWA. 2009. In Vivo Dynamics of Intracistronic Transcriptional Polarity. *Journal of Molecular Biology* **385**:733–747. doi:10.1016/j.jmb.2008.11.020

de Smit MH, Verlaan PWG, van Duin J, Pleij CWA. 2008. Intracistronic transcriptional polarity enhances translational repression: a new role for Rho. *Molecular microbiology* **69**:1278–89.

Deana A, Belasco JG. 2005. Lost in translation: the influence of ribosomes on bacterial mRNA decay. *Genes Dev* **19**:2526–2533. doi:10.1101/gad.1348805

D'Halluin A, Polgar P, Kipkorir T, Patel Z, Cortes T, Arnvig KB. 2022. Term-seq reveals an abundance of conditional, Rho-dependent termination in Mycobacterium tuberculosis. doi:10.1101/2022.06.01.494293

Dornenburg JE, Devita AM, Palumbo MJ, Wade JT. 2010. Widespread antisense transcription in Escherichia coli. *mBio* **1**. doi:10.1128/mBio.00024-10

Dzyubak E, Yap M-NF. 2016. The expression of antibiotic resistance methyltransferase correlates with mRNA stability independently of ribosome stalling. *Antimicrobial Agents and Chemotherapy* **60**:AAC.01806-16. doi:10.1128/AAC.01806-16

Feinberg JS, Joseph S. 2006. A Conserved Base-pair between tRNA and 23 S rRNA in the Peptidyl Transferase Center Is Important for Peptide Release. *Journal of Molecular Biology*. doi:10.1016/j.jmb.2006.09.040

Fostier CR, Ousalem F, Leroy EC, Ngo S, Soufari H, Innis CA, Hashem Y, Boël G. 2023. Regulation of the macrolide resistance ABC-F translation factor MsrD. *Nat Commun* **14**:3891. doi:10.1038/s41467-023-39553-8

Gregory ST, Lieberman KR, Dahlberg AE. 1994. Mutations in the peptidyl transferase region of E. coli 23S rRNA affecting translational accuracy. *Nucleic acids research* **22**:279–84.

Herrero Del Valle A, Seip B, Cervera-Marzal I, Sacheau G, Seefeldt AC, Innis CA. 2020. Ornithine capture by a translating ribosome controls bacterial polyamine synthesis. *Nat Microbiol* **5**:554–561. doi:10.1038/s41564-020-0669-1

Hirabayashi N, Sato NS, Suzuki T. 2006. Conserved loop sequence of helix 69 in Escherichia coli 23 S rRNA is involved in A-site tRNA binding and translational fidelity. *The Journal of biological chemistry* **281**:17203–11. doi:10.1074/jbc.M511728200

Horton RM, Cai ZL, Ho SN, Pease LR. 1990. Gene splicing by overlap extension: tailor-made genes using the polymerase chain reaction. *BioTechniques* **8**:528–535.

Kahlmeter G, Turnidge J. 2022. How to: ECOFFs-the why, the how, and the don’ts of EUCAST epidemiological cutoff values. *Clin Microbiol Infect* **28**:952–954. doi:10.1016/j.cmi.2022.02.024

Kipper K, Hetényi C, Sild S, Remme J, Liiv A. 2009. Ribosomal intersubunit bridge B2a is involved in factor-dependent translation initiation and translational processivity. *J Mol Biol* **385**:405–422. doi:10.1016/j.jmb.2008.10.065

Kipper K, Sild S, Hetényi C, Remme J, Liiv A. 2011. Pseudouridylation of 23S rRNA helix 69 promotes peptide release by release factor RF2 but not by release factor RF1. *Biochimie*. doi:10.1016/j.biochi.2010.12.018

Kohanski MA, Dwyer DJ, Wierzbowski J, Cottarel G, Collins JJ. 2008. Mistranslation of membrane proteins and two-component system activation trigger antibiotic-mediated cell death. *Cell* **135**:679–90. doi:10.1016/j.cell.2008.09.038

Kriner MA, Groisman EA. 2017. RNA secondary structures regulate three steps of Rho-dependent transcription termination within a bacterial mRNA leader. *Nucleic Acids Research* **45**:631–642. doi:10.1093/nar/gkw889

Kriner MA, Sevostyanova A, Groisman EA. 2016. Learning from the Leaders: Gene Regulation by the Transcription Termination Factor Rho. *Trends in biochemical sciences* **41**:690–699. doi:10.1016/j.tibs.2016.05.012

Landick R, Yanofsky C. 1987. Transcription Attenuation. *American Society for Microbiology* **1**:1276–1301.

Lange C, Lehr M, Zerulla K, Ludwig P, Schweitzer J, Polen T, Wendisch VF, Soppa J. 2017. Effects of Kasugamycin on the Translatome of Escherichia coli. *PLoS One* **12**:e0168143. doi:10.1371/journal.pone.0168143

Lee J-H, Lee E-J, Roe J-H. 2022. uORF-mediated riboregulation controls transcription of whiB7/wblC antibiotic resistance gene. *Molecular Microbiology* **117**:179–192. doi:10.1111/mmi.14834

Lee SK, Keasling JD. 2005. A propionate-inducible expression system for enteric bacteria. *Applied and environmental microbiology*. doi:10.1128/AEM.71.11.6856-6862.2005

Li SC, Squires CL, Squires C. 1984. Antitermination of E. coli rRNA transcription is caused by a control region segment containing lambda nut-like sequences. *Cell* **38**:851–60.

Liiv A, Karitkina D, Maiväli Ü, Remme J. 2005. Analysis of the function of E. coli 23S rRNA helix-loop 69 by mutagenesis. *BMC Molecular Biology*. doi:10.1186/1471-2199-6-18

Love MI, Huber W, Anders S. 2014. Moderated estimation of fold change and dispersion for RNA-seq data with DESeq2. *Genome biology* **15**:550. doi:10.1186/s13059-014-0550-8

Lybecker M, Zimmermann B, Bilusic I, Tukhtubaeva N, Schroeder R. 2014. The double-stranded transcriptome of Escherichia coli. *Proc Natl Acad Sci U S A* **111**:3134–3139. doi:10.1073/pnas.1315974111

Madeira F, Pearce M, Tivey ARN, Basutkar P, Lee J, Edbali O, Madhusoodanan N, Kolesnikov A, Lopez R. 2022. Search and sequence analysis tools services from EMBL-EBI in 2022. *Nucleic Acids Res* **50**:W276–W279. doi:10.1093/nar/gkac240

Mao X, Ma Q, Liu B, Chen X, Zhang H, Xu Y. 2015. Revisiting operons: an analysis of the landscape of transcriptional units in E. coli. *BMC Bioinformatics* **16**:356. doi:10.1186/s12859-015-0805-8

Marks J, Kannan K, Roncase EJ, Klepacki D, Kefi A, Orelle C, Vázquez-Laslop N, Mankin AS. 2016. Context-specific inhibition of translation by ribosomal antibiotics targeting the peptidyl transferase center. *Proceedings of the National Academy of Sciences* **113**:12150–12155. doi:10.1073/pnas.1613055113

Martinez A, Opperman T, Richardson JP. 1996. Mutational analysis and secondary structure model of the RNP1-like sequence motif of transcription termination factor Rho. *Journal of Molecular Biology* **257**:895–908. doi:10.1006/jmbi.1996.0210

Matsumoto Y, Shigesada K, Hirano M, Imai M. 1986. Autogenous regulation of the gene for transcription termination factor rho in Escherichia coli: localization and function of its attenuators. *Journal of bacteriology* **166**:945–58.

McClure R, Balasubramanian D, Sun Y, Bobrovskyy M, Sumby P, Genco CA, Vanderpool CK, Tjaden B. 2013. Computational analysis of bacterial RNA-Seq data. *Nucleic Acids Res* **41**:e140.

McGaha SM, Champney WS. 2007. Hygromycin B inhibition of protein synthesis and ribosome biogenesis in Escherichia coli. *Antimicrob Agents Chemother* **51**:591–596. doi:10.1128/AAC.01116-06

Meydan S, Marks J, Klepacki D, Sharma V, Baranov PV, Firth AE, Margus T, Kefi A, Vázquez-Laslop N, Mankin AS. 2019. Retapamulin-Assisted Ribosome Profiling Reveals the Alternative Bacterial Proteome. *Molecular Cell* **74**:481–493. doi:10.1016/j.molcel.2019.02.017

Nadiras C, Eveno E, Schwartz A, Figueroa-Bossi N, Boudvillain M. 2018. A multivariate prediction model for Rho-dependent termination of transcription. *Nucleic Acids Research* **46**:8245–8260. doi:10.1093/nar/gky563

Nakahigashi K, Takai Y, Kimura M, Abe N, Nakayashiki T, Shiwa Y, Yoshikawa H, Wanner BL, Ishihama Y, Mori H. 2016. Comprehensive identification of translation start sites by tetracycline-inhibited ribosome profiling. *DNA Research* **23**:193–201. doi:10.1093/dnares/dsw008

Nguyen F, Starosta AL, Arenz S, Sohmen D, Dönhöfer A, Wilson DN. 2014. Tetracycline antibiotics and resistance mechanisms. *Biol Chem* **395**:559–575. doi:10.1515/hsz-2013-0292

Obana N, Takada H, Crowe-McAuliffe C, Iwamoto M, Egorov AA, Wu KJY, Chiba S, Murina V, Paternoga H, Tresco BIC, Nomura N, Myers AG, Atkinson GC, Wilson DN, Hauryliuk V. 2023. Genome-encoded ABCF factors implicated in intrinsic antibiotic resistance in Gram-positive bacteria: VmlR2, Ard1 and CplR. *Nucleic Acids Res* gkad193. doi:10.1093/nar/gkad193

Orelle C, Carlson S, Kaushal B, Almutairi MM, Liu H, Ochabowicz A, Quan S, Pham VC, Squires CL, Murphy BT, Mankin AS. 2013. Tools for Characterizing Bacterial Protein Synthesis Inhibitors. *Antimicrobial Agents and Chemotherapy* **57**:5994–6004. doi:10.1128/AAC.01673-13

Osterman IA, Prokhorova IV, Sysoev VO, Boykova YV, Efremenkova OV, Svetlov MS, Kolb VA, Bogdanov AA, Sergiev PV, Dontsova OA. 2012. Attenuation-based dual-fluorescent-protein reporter for screening translation inhibitors. *Antimicrob Agents Chemother* **56**:1774–1783. doi:10.1128/AAC.05395-11

Page R, Peti W. 2016. Toxin-antitoxin systems in bacterial growth arrest and persistence. *Nature Chemical Biology* **12**:208–214. doi:10.1038/nchembio.2044

Peters JM, Mooney RA, Grass JA, Jessen ED, Tran F, Landick R. 2012. Rho and NusG suppress pervasive antisense transcription in Escherichia coli. *Genes & development* **26**:2621–33. doi:10.1101/gad.196741.112

Peters JM, Mooney RA, Kuan PF, Rowland JL, Keles S, Landick R. 2009. Rho directs widespread termination of intragenic and stable RNA transcription. *Proceedings of the National Academy of Sciences of the United States of America* **106**:15406–11. doi:10.1073/pnas.0903846106

Ramu H, Mankin A, Vazquez-Laslop N. 2009. Programmed drug-dependent ribosome stalling: MicroReview. *Molecular Microbiology* **71**:811–824. doi:10.1111/j.1365-2958.2008.06576.x

Richardson JP. 2002. Rho-dependent termination and ATPases in transcript termination. *Biochimica et biophysica acta* **1577**:251–260.

Rivellini F, Alifano P, Piscitelli C, Blasi V, Bruni CB, Carlomagno MS, Brunt CB, Carlomagno MS. 1991. A cytosine- over guanosine-rich sequence in RNA activates rho-dependent transcription termination. *Molecular Microbiology* **5**:3049–3054. doi:10.1111/j.1365-2958.1991.tb01864.x

Samaha RR, Green R, Noller HF. 1995. A base pair between tRNA and 23S rRNA in the peptidyl transferase centre of the ribosome. *Nature* **377**:309–314. doi:10.1038/377309a0

Schneider D, Gold L, Platt T. 1993. Selective Enrichment of Rna Species for Tight-Binding to Escherichia-Coli Rho-Factor. *Faseb Journal* **7**:201–207.

Schwartz A, Walmacq C, Rahmouni AR, Boudvillain M. 2007. Noncanonical interactions in the management of RNA structural blocks by the transcription termination rho helicase. *Biochemistry* **46**:9366–79. doi:10.1021/bi700493m

Seemann SE, Gorodkin J, Backofen R. 2008. Unifying evolutionary and thermodynamic information for RNA folding of multiple alignments. *Nucleic Acids Res* **36**:6355–6362. doi:10.1093/nar/gkn544

Seemann SE, Menzel P, Backofen R, Gorodkin J. 2011. The PETfold and PETcofold web servers for intra- and intermolecular structures of multiple RNA sequences. *Nucleic Acids Res* **39**:W107-111. doi:10.1093/nar/gkr248

Seip B, Innis CA. 2016. How Widespread is Metabolite Sensing by Ribosome-Arresting Nascent Peptides? *Journal of Molecular Biology* **428**:2217–2227. doi:10.1016/j.jmb.2016.04.019

Shaw KJ, Miller N, Liu X, Lerner D, Wan J, Bittner A, Morrow BJ. 2003. Comparison of the changes in global gene expression of Escherichia coli induced by four bactericidal agents. *J Mol Microbiol Biotechnol* **5**:105–122. doi:10.1159/000069981

Shong J, Collins CH. 2013. Engineering the esaR promoter for tunable quorum sensing- dependent gene expression. *ACS synthetic biology* **2**:568–75. doi:10.1021/sb4000433

Singh N, Bubunenko M, Smith C, Abbott DM, Stringer AM, Shi R, Court DL, Wade JT. 2016. SuhB Associates with Nus Factors To Facilitate 30S Ribosome Biogenesis in Escherichia coli. *mBio* **7**. doi:10.1128/mBio.00114-16

Smith C, Canestrari JG, Wang AJ, Champion MM, Derbyshire KM, Gray TA, Wade JT. 2022. Pervasive translation in Mycobacterium tuberculosis. *Elife* **11**:e73980. doi:10.7554/eLife.73980

Stringer A, Smith C, Mangano K, Wade JT. 2021. Identification of novel translated small ORFs in Escherichia coli using complementary ribosome profiling approaches. *J Bacteriol* JB0035221. doi:10.1128/JB.00352-21

Stringer AM, Currenti S, Bonocora RP, Baranowski C, Petrone BL, Palumbo MJ, Reilly AA, Zhang Z, Erill I, Wade JT. 2014. Genome-scale analyses of Escherichia coli and Salmonella enterica AraC reveal noncanonical targets and an expanded core regulon. *Journal of bacteriology* **196**:660–71. doi:10.1128/JB.01007-13

Stringer AM, Singh N, Yermakova A, Petrone BL, Amarasinghe JJ, Reyes-Diaz L, Mantis NJ, Wade JT. 2012. FRUIT, a scar-free system for targeted chromosomal mutagenesis, epitope tagging, and promoter

replacement in Escherichia coli and Salmonella enterica. *PloS one* **7**:e44841. doi:10.1371/journal.pone.0044841

Subramanian SL, Ramu H, Mankin AS. 2012. Inducible resistance to macrolide antibioticsAntibiotic Discovery and Development. Boston, MA: Springer US. pp. 455–484. doi:10.1007/978-1-4614-1400-1_13

Suvorov AN, van Gemen B, van Knippenberg PH. 1988. Increased kasugamycin sensitivity in Escherichia coli caused by the presence of an inducible erythromycin resistance (erm) gene of Streptococcus pyogenes. *Mol Gen Genet* **215**:152–155. doi:10.1007/BF00331317

Syroegin EA, Flemmich L, Klepacki D, Vazquez-Laslop N, Micura R, Polikanov YS. 2022. Structural basis for the context-specific action of the classic peptidyl transferase inhibitor chloramphenicol. *Nat Struct Mol Biol* **29**:152–161. doi:10.1038/s41594-022-00720-y

Takada H, Mandell ZF, Yakhnin H, Glazyrina A, Chiba S, Kurata T, Wu KJY, Tresco BIC, Myers AG, Aktinson GC, Babitzke P, Hauryliuk V. 2022. Expression of Bacillus subtilis ABCF antibiotic resistance factor VmlR is regulated by RNA polymerase pausing, transcription attenuation, translation attenuation and (p)ppGpp. *Nucleic Acids Res* **50**:6174–6189. doi:10.1093/nar/gkac497

Thomason MK, Bischler T, Eisenbart SK, Förstner KU, Zhang A, Herbig A, Nieselt K, Sharma CM, Storz G. 2015. Global Transcriptional Start Site Mapping Using Differential RNA Sequencing Reveals Novel Antisense RNAs in Escherichia coli. *Journal of Bacteriology* **197**:18–28. doi:10.1128/JB.02096-14

van der Stel A-X, Gordon ER, Sengupta A, Martínez AK, Klepacki D, Perry TN, Herrero Del Valle A, Vázquez-Laslop N, Sachs MS, Cruz-Vera LR, Innis CA. 2021. Structural basis for the tryptophan sensitivity of TnaC-mediated ribosome stalling. *Nat Commun* **12**:5340. doi:10.1038/s41467-021-25663-8

Vázquez-Laslop N, Mankin AS. 2018a. Context-Specific Action of Ribosomal Antibiotics. *Annual Review of Microbiology* **72**:185–207. doi:10.1146/annurev-micro-090817-062329

Vázquez-Laslop N, Mankin AS. 2018b. How Macrolide Antibiotics Work. *Trends Biochem Sci* **43**:668–684. doi:10.1016/j.tibs.2018.06.011

Venturini E, Svensson SL, Maaß S, Gelhausen R, Eggenhofer F, Li L, Cain AK, Parkhill J, Becher D, Backofen R, Barquist L, Sharma CM, Westermann AJ, Vogel J. 2020. A global data-driven census of Salmonella small proteins and their potential functions in bacterial virulence. *microLife* **1**. doi:10.1093/femsml/uqaa002

Vimberg V, Cavanagh JP, Novotna M, Lenart J, Nguyen Thi Ngoc B, Vesela J, Pain M, Koberska M, Balikova Novotna G. 2020. Ribosome-Mediated Attenuation of vga(A) Expression Is Shaped by the Antibiotic Resistance Specificity of Vga(A) Protein Variants. *Antimicrob Agents Chemother* **64**:e00666-20. doi:10.1128/AAC.00666-20

Wang J, Rennie W, Liu C, Carmack CS, Prévost K, Caron M-P, Massé E, Ding Y, Wade JT. 2015. Identification of bacterial sRNA regulatory targets using ribosome profiling. *Nucleic acids research* **43**:10308–20. doi:10.1093/nar/gkv1158

Wang Y, Rotman ER, Shoemaker NB, Salyers AA. 2005. Translational Control of Tetracycline Resistance and Conjugation in the Bacteroides Conjugative Transposon CTnDOT. *Journal of Bacteriology* **187**:2673–2680. doi:10.1128/JB.187.8.2673-2680.2005

Watters KE, Abbott TR, Lucks JB. 2016a. Simultaneous characterization of cellular RNA structure and function with in-cell SHAPE-Seq. *Nucleic Acids Research* **44**:e12. doi:10.1093/nar/gkv879

Watters KE, Yu AM, Strobel EJ, Settle AH, Lucks JB. 2016b. Characterizing RNA structures in vitro and in vivo with selective 2’-hydroxyl acylation analyzed by primer extension sequencing (SHAPE-Seq). *Methods* **103**:34–48. doi:10.1016/j.ymeth.2016.04.002

Weaver J, Mohammad F, Buskirk AR, Storz G. 2019. Identifying Small Proteins by Ribosome Profiling with Stalled Initiation Complexes. *mBio* **10**. doi:10.1128/mBio.02819-18

Yakhnin H, Babiarz JE, Yakhnin AV, Babitzke P. 2001. Expression of the Bacillus subtilis trpEDCFBA operon is influenced by translational coupling and Rho termination factor. *J Bacteriol* **183**:5918–5926. doi:10.1128/JB.183.20.5918-5926.2001

Yakhnin H, Yakhnin AV, Mouery BL, Mandell ZF, Karbasiafshar C, Kashlev M, Babitzke P. 2019. NusG-Dependent RNA Polymerase Pausing and Tylosin-Dependent Ribosome Stalling Are Required for

Tylosin Resistance by Inducing 23S rRNA Methylation in Bacillus subtilis. *mBio* **10**:e02665-19. doi:10.1128/mBio.02665-19

Yamaguchi Y, Inouye M. 2015. An endogenous protein inhibitor, YjhX (TopAI), for topoisomerase i from Escherichia coli. *Nucleic Acids Research* **43**:10387–10396. doi:10.1093/nar/gkv1197

Yan K, Madden L, Choudhry AE, Voigt CS, Copeland RA, Gontarek RR. 2006. Biochemical characterization of the interactions of the novel pleuromutilin derivative retapamulin with bacterial ribosomes. *Antimicrobial Agents and Chemotherapy* **65**:232–260. doi:10.1128/AAC.00184-06

Yang Y, Xiao T, Li J, Cheng P, Li F, Yu H, Liu R, Muhammad I, Zhang X. 2020. Wild-type cutoff for Apramycin against Escherichia coli. *BMC Vet Res* **16**:309. doi:10.1186/s12917-020-02522-0

Zuker M. 2003. Mfold web server for nucleic acid folding and hybridization prediction. *Nucleic acids research* **31**:3406–15.

FIGURE LEGENDS

Figure 1. Rho-dependent transcription termination within the *topAI* gene. (A) Schematic representation of the *E. coli topAI-yjhQ-yjhP* operon, including the *toiL* uORF. **(B)** Schematic representation of *topAI-lacZ* transcriptional reporter fusions, indicating the position of the transcription start site (TSS) with respect to the *topAI* start codon, and the mutation in the putative *rut*. **(C)** β-galactosidase activity of *topAI-lacZ* transcriptional fusions in wild-type (strain AMD054) or *rho* mutant (R66S amino acid substitution in Rho; strain GB004) cells. Reporter fusions with wild-type sequence or mutation of the predicted *rut* (*rut**) extend to position +42 or +10 of *topAI* (wild-type +42, plasmid pGB217; wild-type +10, plasmid pGB215; *rut** +42, plasmid pGB306; *rut** +10, plasmid pGB305). Error bars represent ±1 standard deviation from the mean (n = 3).

Figure 2. *topAI* expression is induced in response to translation stress. (A) Schematic representation of *topAI-lux* translational reporter fusions, indicating the position of the *toiL* start codon with respect to the *topAI* start codon. **(B)** Luciferase activity of the wild-type *topAI-lux* translational reporter fusion (pGB202) in Δ*topAI-yjhQ* cells (strain GB001) expressing either wild-type 23S rRNA (plasmid pGB322) or ΔT1917 23S rRNA (plasmid pGB318) in *trans*. Activity was measured four hours post-induction with propionate. **(C)** Luciferase activity of wild-type and mutant *topAI-lux* translational reporter fusions in Δ*topAI-yjhQ* cells (strain GB001) grown in the presence of ribosome-targeting antibiotics. Cells were grown in LB medium to an OD_{600} of ~1.0. Indicated samples were treated with tetracycline (0.5 μg/ml), spectinomycin (90 μg/ml), retapamulin (4 μg/ml), erythromycin (100 μg/ml), tylosin (400 μg/ml), or chloramphenicol (1 μg/ml). Luminescence was measured 90 min after antibiotic treatment. Error bars represent ±1 standard deviation from the mean (n = 3).

Figure 2, Figure Supplement 1. *topAI* is translationally repressed. (A) Schematic representation of the *topAI-lux* translational reporter fusion. **(B)** Luciferase activity of the *topAI-lux* translational fusion (plasmid pGB202) in Δ*topAI-yjhQ* cells ("Wild-type"; strain GB001) or in Δ*topAI-yjhQ rho* mutant (R66S amino acid substitution in Rho; strain GB004). Error bars represent ±1 standard deviation from the mean (n = 3).

Figure 3. Tetracycline treatment reduces premature Rho-dependent transcription termination within *topAI-yjhQ* and increases abundance of the associated mRNA. (A) Schematic of the *rhoL-rho* and *topAI-yjhQP* operons showing the positions of PCR amplicons used for ChIP-qPCR and/or qRT-PCR. **(B)** Occupancy of RNAP measured by ChIP-qPCR in the *rho* gene. Occupancy values are normalized to those in *rhoL* (control PCR amplicon "C" in panel A). Data are shown for wild-type (strain MG1655) or *rho* mutant (R66S amino acid substitution in Rho; strain CRB016) cells grown in the presence or absence of tetracycline, as indicated. The *x*-axis label corresponds to the PCR amplicon shown in panel A. **(C)** Occupancy of RNAP measured by ChIP-qPCR at positions across the *topAI-yjhQ* transcript. Occupancy values are normalized to those in the *topAI* upstream region (control PCR amplicon "C" in panel A). **(D)** RNA levels measured by qRT-PCR at positions across the *topAI-yjhQ* transcript, normalized to the *mreB* gene. Error bars represent ±1 standard deviation from the mean (n = 3). Statistical significance is indicated as follows: n.s. = not significant ($p > 0.05$), * $p < 0.05$, ** $p < 0.01$, *** $p < 0.001$.

Figure 4. A uORF, *toiL*, is located within the *topAI* 5' upstream region. (A) Schematic representation of *toiL-lacZ* translational reporter fusions, indicating mutations upstream and within the

toiL uORF. **(B)** β-galactosidase activity of the wild-type *toiL-lacZ* translational reporter fusion (wt; plasmid pGB164), and fusions with mutations immediately upstream of *toiL* (TTG→tga; plasmid pGB201), at the *toiL* start codon (ATG→tga; plasmid pGB200), second codon (CTG→tga; plasmid pGB197), or fourth codon (AAT→tga; plasmid pGB196), in cells with wild-type *topAI-yjhQP* (strain AMD054). Error bars represent ±1 standard deviation from the mean (n = 3).

Figure 4, Figure Supplement 1. ToiL conservation across *Enterobacteriaceae* species. Predicted ToiL sequences were aligned with ClustalO (Madeira et al., 2022). Asterisks indicate fully conserved positions.

Figure 5. *toiL* translation is required for induction of *topAI* expression by ribosome-targeting antibiotics. (A) Schematic representation of *topAI-lux* translational reporter fusions, indicating mutations in the start codon and Shine-Dalgarno sequence of the *toiL* uORF. **(B)** Luciferase activity of wild-type and mutant *topAI-lux* translational reporter fusions in Δ*topAI-yjhQ* cells (strain GB001) grown in the presence of ribosome-targeting antibiotics. Cells were grown as indicated in Figure 2C. Dark gray bars show data for the wild-type *topAI-lux* translational reporter fusion (plasmid pGB202); light gray bars show data for the *topAI-lux* translational reporter fusion with a mutated *toiL* start codon (plasmid pGB313); white bars show data for the *topAI-lux* translational reporter fusion with a mutated *toiL* Shine-Dalgarno sequence (pGB366). Note that data for the wild-type *topAI-lux* translational reporter fusion are identical to those in Figure 2C and are included here for reference. Error bars represent ±1 standard deviation from the mean (n = 3).

Figure 5, Figure Supplement 1. Mutation of the *toiL* start codon does not alter predicted RNA secondary structure and does not lead to Rho-dependent transcription termination in the *topAI* 5' upstream region. (A) Predicted minimum free-energy secondary structures of the *topAI* 5' UR for wild-type sequence and sequence where the *toiL* start codon (ATG) is mutated (GTA). **(B)** Schematic representation of *topAI-lacZ* transcriptional reporter fusions indicating the start codon mutation of *toiL*. **(C)** β-galactosidase activity of the wild-type *topAI-lacZ* transcriptional reporter (plasmid pGB182) and the *toiL* start codon mutant reporter (plasmid pGB297) in Δ*topAI-yjhQ* cells (strain GB001). Error bars represent ±1 standard deviation from the mean (n = 3).

Figure 6. Structural changes in the *topAI* 5′ upstream region induced by tetracycline treatment. (A) Predicted RNA secondary structure of the *topAI* 5' UR, indicating in-cell SHAPE reactivities of each base from an untreated sample. Values of ρ are indicated on a color gradient. The position of the *toiL* uORF is indicated by a red arrow, and the position of the start of *topAI* is indicated by a gray rectangle. Numbers indicate position relative to the mRNA 5' end. **(B)** In-cell SHAPE reactivities of each base from three replicates of untreated samples and two replicates of tetracycline-treated samples. SHAPE reacrtivity values are indicated on the same color gradient as panel A. Nucleotide positions with statistically significant differences ($p < 0.01$ or 0.05, as indicated) in SHAPE reactivity between untreated and tetracycline-treated samples are indicated by red (lower reactivity in tetracycline-treated samples) or green (higher reactivity in tetracycline-treated samples) squares.

Figure 6, Figure Supplement 1. Predicted RNA secondary structure for the *topAI* upstream region based on sequence conservation (A) PETfold alignment of *topAI* 5' UR sequences from selected species. Predicted base pairing interactions are represented in a dot-bracket format below the alignment.

Reliability of base pairing (reliab_paired) and sequence conservation scores are represented as grey bars (0 - 1 scale). **(B)** Representation of the PETfold-predicted *topAI* 5' UR RNA consensus structure. Nucleotide colors in both panels follow the Vienna RNA conservation coloring schema (Bernhart et al., 2008) and represent the number of compatible or incompatible nucleotide pairs for each position, as indicated.

Figure 7. Tetracycline stalls ribosomes on start codons. (A) Normalized Ribo-seq coverage for all annotated ORFs for cells (strain MG1655) grown ± tetracycline. **(B)** Heatmap showing normalized Ribo-seq coverage in the region around the *toiL* uORF in untreated cells (no antibiotic) or tetracycline-treated cells. The color indicates the sequence-read coverage for RNA fragment 3' ends that are presumed to represent the downstream edge of ribosome footprints. The *toiL* uORF position and encoded amino acid sequence is indicated. **(C)** Average of normalized Ribo-seq coverage for the regions around start codons for all annotated ORFs, for untreated cells (gray line; no antibiotic) or tetracycline-treated cells (orange line). Sequence-read coverage was calculated for RNA fragment 3' ends that are presumed to represent the downstream edge of ribosome footprints.

Figure 8. Ribosome stalling at the *topAI* leader *in vivo*. (A) Schematic showing the *toiL-ermCL-lux* stalling reporter in the translationally inactive conformation ("OFF") that is expected in the absence of ribosome stalling, and the translationally active conformation ("ON") that is expected when ribosomes stall within *toiL* sequence close to the junction of *toiL* with *ermCL*. **(B)** Schematic showing *toiL-ermCL* stalling reporters where *toiL* is progressively extended by one codon at the 3' end and fused to part of *ermCL*. *toiL* sequence is indicated by red arrows; *ermCL* sequence is indicated by green arrows. The last indicated stalling reporter extends to position 5 of *toiL* but has a Val5→Leu substitution (blue). **(C)**

Luciferase activity of the *toiL-ermCL-lux* stalling reporters (plasmids pGB323, pGB346, pGB325, pGB326, pGB324, pGB328, pGB329, pGB307, pGB347, and pGB327) in Δ*topAI-yjhQ* cells (strain GB001). Cells were grown to an OD_{600} of ~1.0 and treated with the indicated ribosome-targeting antibiotics at the same concentrations as in Figure 2C. Luminescence was measured three hours post-treatment. Horizontal dashed lines indicate luminescence activity of 1, to facilitate comparison between panels with different *y*-axis scales. Error bars represent ±1 standard deviation from the mean (n = 3).

Figure 8, Figure Supplement 1. Predicted RNA structures for translationally inactive and active conformations of *toiL* stalling reporters. Predicted RNA structures are shown for *toiL-ermCL-lux* stalling reporters where increasing lengths of *toiL* are fused to part of *ermCL*. *toiL* is indicated by red arrows. *ermCL* sequence is indicated by green arrows. Pausing of ribosomes within *toiL*, close to the junction with *ermCL* sequence, is expected to promote formation of the active ("ON") conformation, whereas the absence of ribosome stalling within *toiL* is expected to promote formation of the inactive ("OFF") conformation.

Figure 8, Figure Supplement 2. Expression of an *ermCL* stalling reporter is specifically induced by erythromycin. (A) Schematic showing the *ermCL-lux* stalling reporter in the translationally inactive conformation ("OFF") that is expected in the absence of erythromycin, when ribosomes do not stall within the *ermCL* uORF; and the translationally active conformation ("ON") that is expected when ribosomes stall within *ermCL* in the presence of erythromycin. **(B)** Predicted RNA secondary structures of the inactive ("OFF") and active ("ON") conformations of the *ermCL-lux* stalling reporter. **(C)** Luciferase activity of the *ermCL-lux* stalling reporter (plasmid pGB308) in Δ*topAI-yjhQ* cells (strain GB001) treated with the indicated ribosome-targeting antibiotics. Cells were grown to an OD_{600} of ~1.0

and treated with the indicated ribosome-targeting antibiotics at the same concentrations as in Figure 2C. Luminescence was measured three hours post-treatment. Error bars represent ±1 standard deviation from the mean (n = 3).

Figure 9. Model for regulation of *topAI* expression. Schematic showing a model for regulation of *topAI* expression. In the repressed state, a hairpin forms between the *toiL* sequence and the ribosome-binding site of *topAI*, repressing translation, which in turn promotes premature Rho-dependent transcription termination within the *topAI* gene. Ribosomes do not stall within *toiL*, so there is minimal perturbation of the repressive hairpin. By contrast, when cells are treated with certain ribosome-targeting antibiotics such as tetracycline, ribosomes stall within *toiL* in a sequence-specific manner, preventing formation of the repressive hairpin.

Figure 1

A

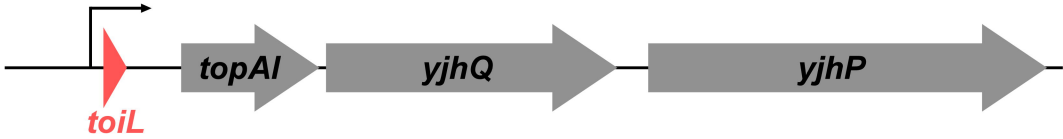
topAI
yjhQ
yjhP
toiL

B

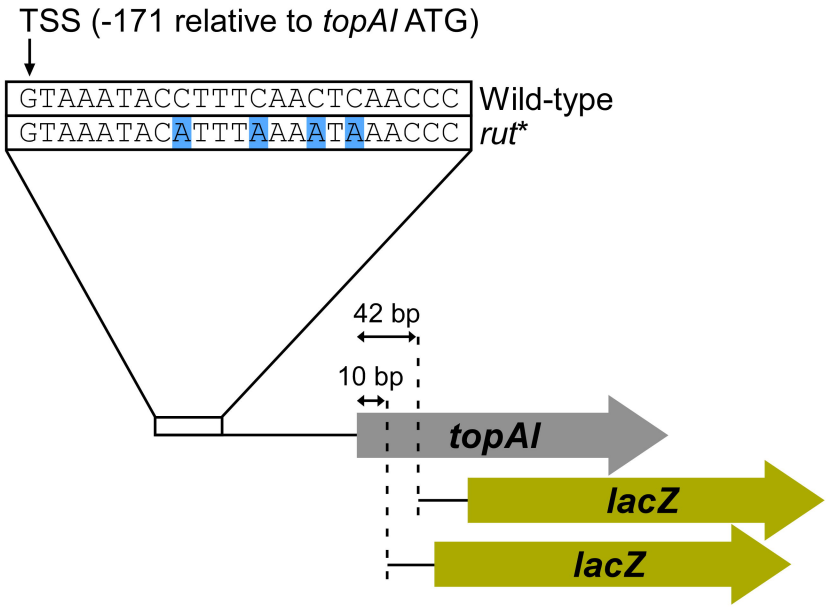
TSS (-171 relative to topAI ATG)
GTAAATACCTTTCAACTCAACCC
Wild-type
GTAAATACATTTAAAATAAACCC
rut*
42 bp
10 bp
topAI
lacZ
lacZ

C

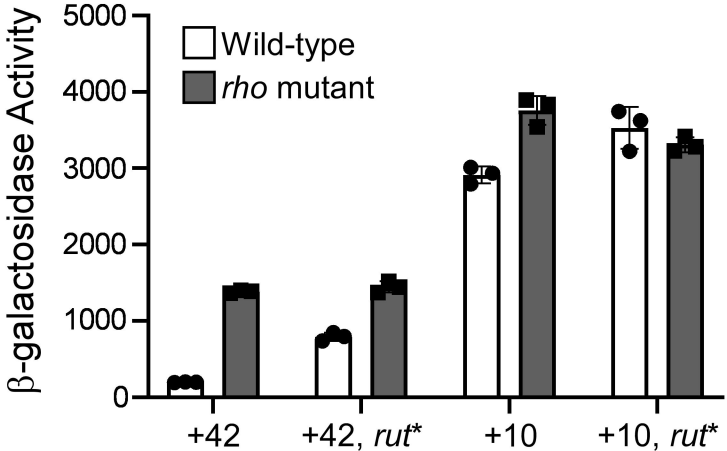
β-galactosidase Activity
5000
4000
3000
2000
1000
0
Wild-type
rho mutant
+42
+42, rut*
+10
+10, rut*

Figure 2

A

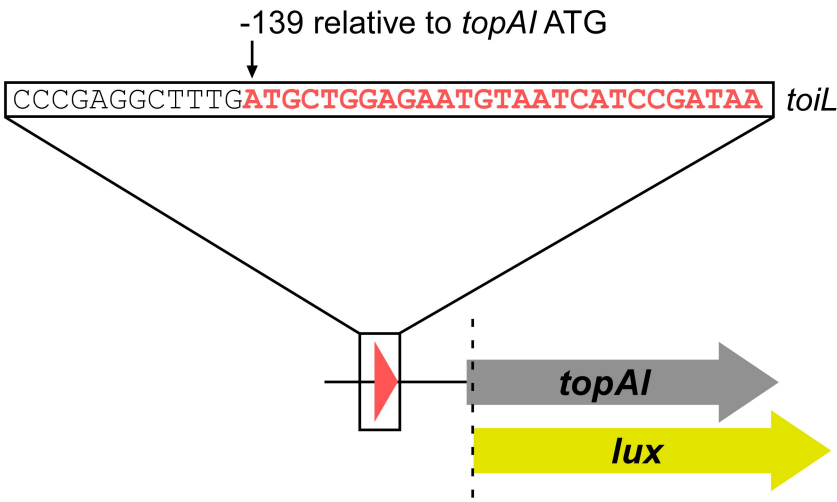
-139 relative to *topAI* ATG
CCCGAGGCTTTGATGCTGGAGAATGTAATCATCCGATAA
toiL
topAI
lux

B

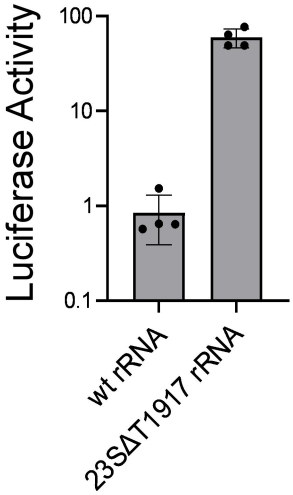
Luciferase Activity
100
10
1
0.1
wt rRNA
23SΔT1917 rRNA

C

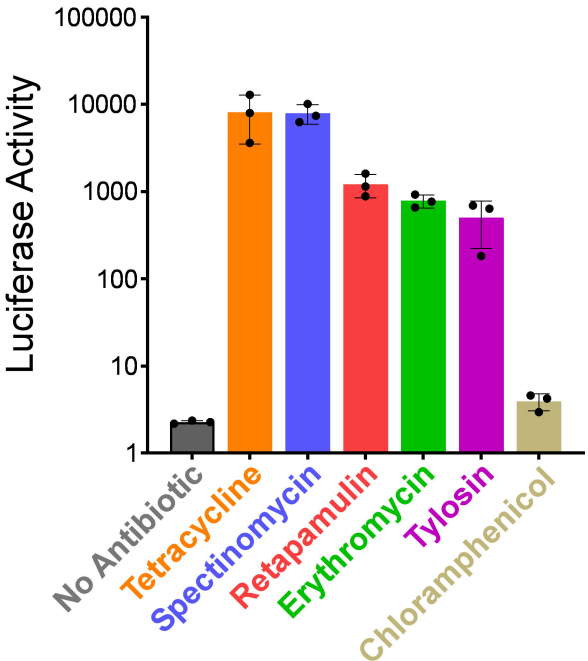
Luciferase Activity
100000
10000
1000
100
10
1
No Antibiotic
Tetracycline
Spectinomycin
Retapamulin
Erythromycin
Tylosin
Chloramphenicol

Figure 2, figure supplement 1

A

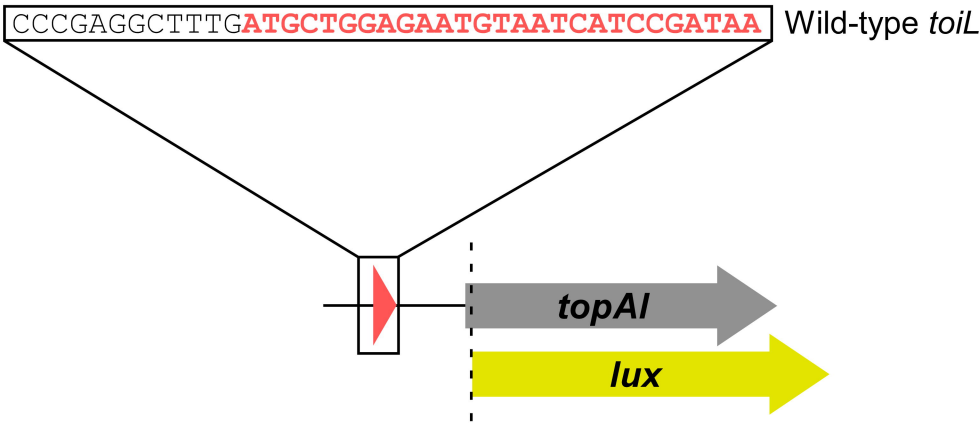

B

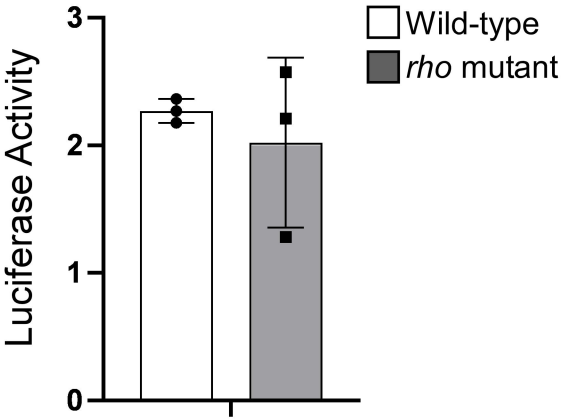

Figure 3

A

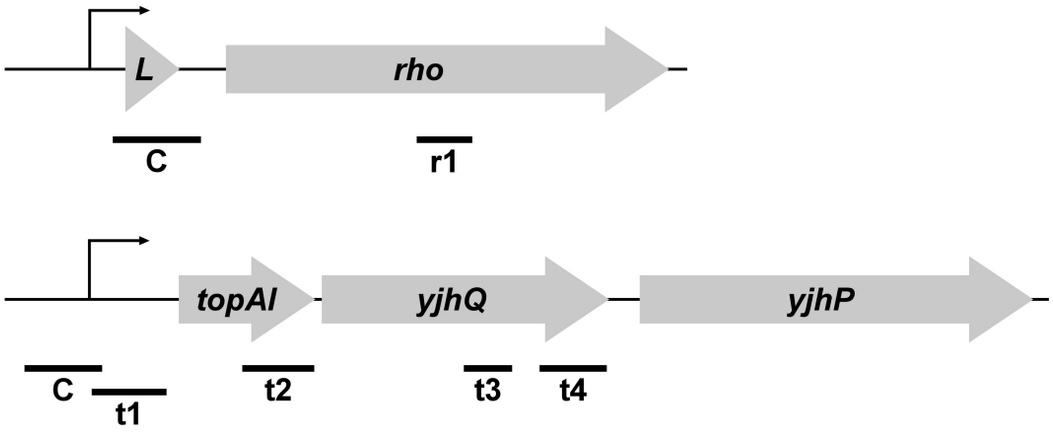

B

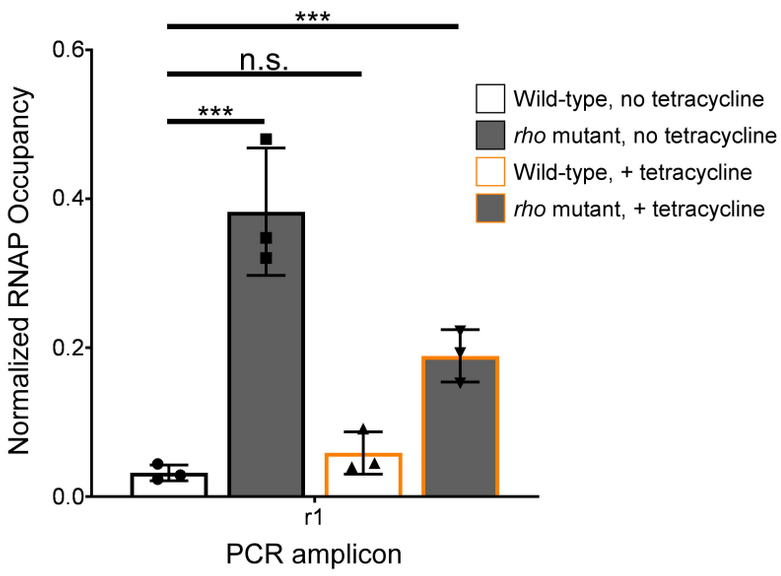

C

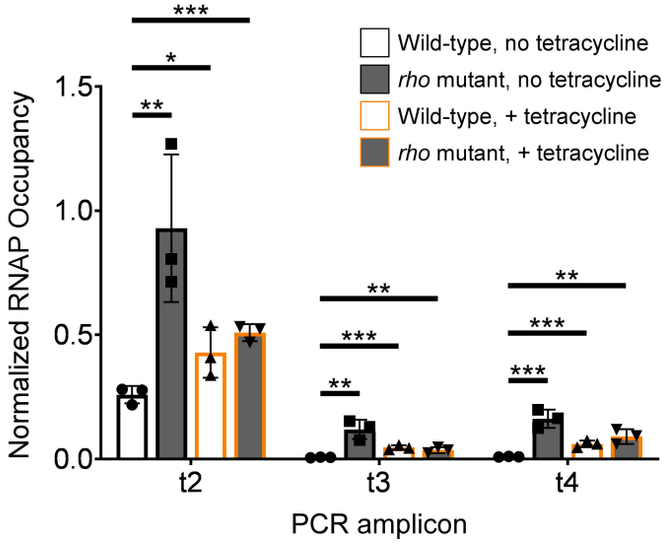

D

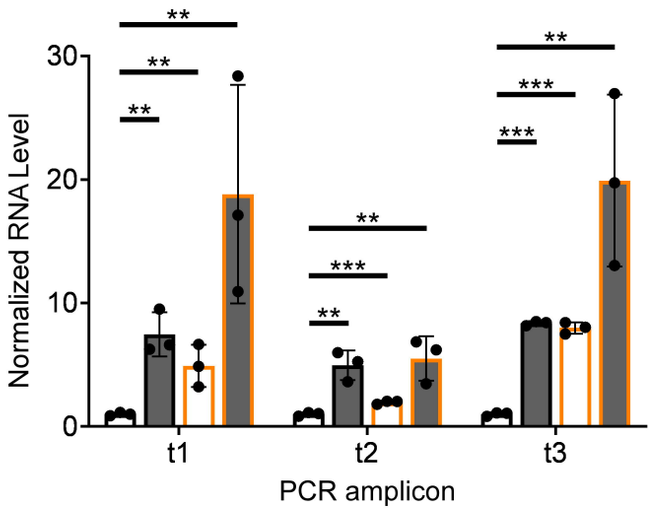

Figure 4

A

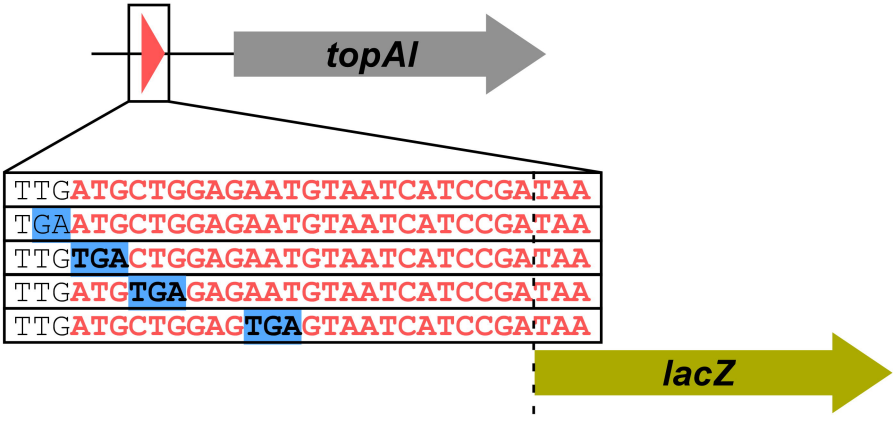
topAI
TTGATGCTGGAGAATGTAATCATCCGATAA
TGAATGCTGGAGAATGTAATCATCCGATAA
TTGTGACTGGAGAATGTAATCATCCGATAA
TTGATGTGAGAGAATGTAATCATCCGATAA
TTGATGCTGGAGTGAGTAATCATCCGATAA
lacZ

B

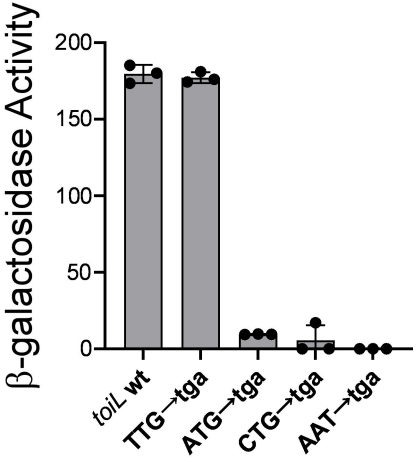
β-galactosidase Activity
200
150
100
50
0
toiL wt
TTG→tga
ATG→tga
CTG→tga
AAT→tga

Figure 4, figure supplement 1

Escherichia coli MG1655	MLENVIIR
Klebsiella pneumoniae RJF293	MLENVIIR
Morganella morganii KT	MLENVIIR
Serratia fonticola GS2	MLENVIIR
Dickeya dadantii 3937	MLENVIIR
Yersinia similis 228	MLENVIIR
Raoultella ornithinolytica B6	MLENVIIG
Enterobacter cloacae ATCC 13047	MLENVII-
Citrobacter amalonaticus Y19	MLENVII-
Salmonella Typhimurium 14028s	MLENVII-
	*******

Figure 5

A

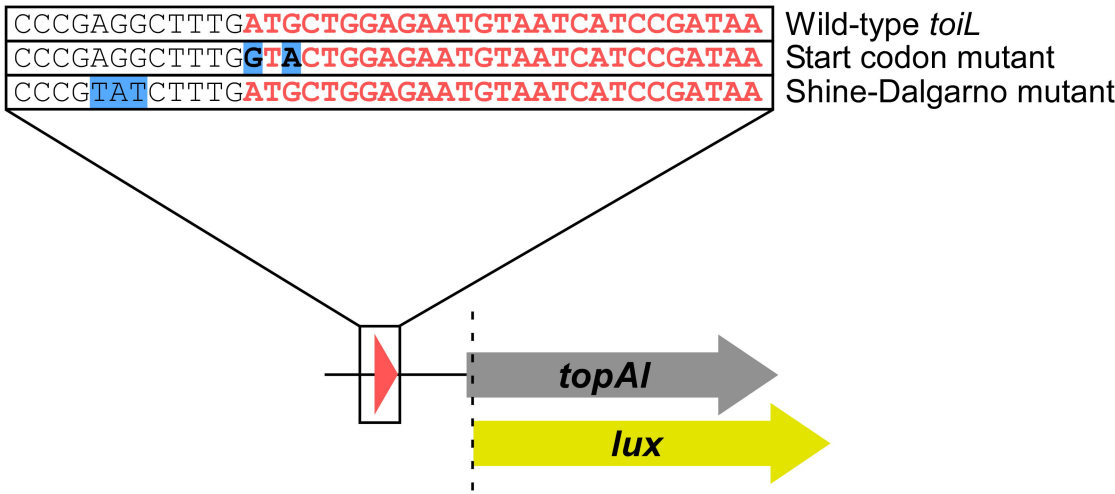
CCCGAGGCTTTGATGCTGGAGAATGTAATCATCCGATAA
Wild-type toiL
CCCGAGGCTTTGGTACTGGAGAATGTAATCATCCGATAA
Start codon mutant
CCCGTATCTTTGATGCTGGAGAATGTAATCATCCGATAA
Shine-Dalgarno mutant
topAI
lux

B

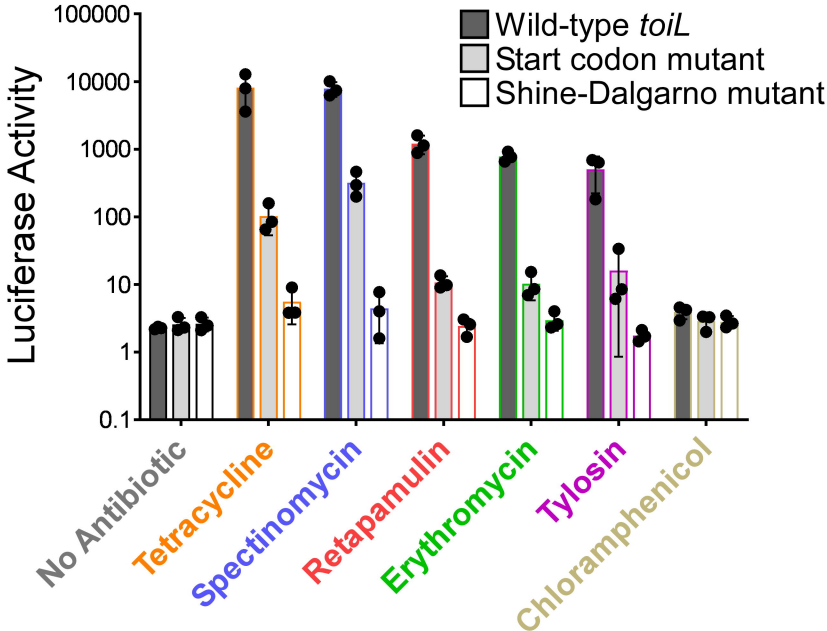
Luciferase Activity
100000
10000
1000
100
10
1
0.1
Wild-type toiL
Start codon mutant
Shine-Dalgarno mutant
No Antibiotic
Tetracycline
Spectinomycin
Retapamulin
Erythromycin
Tylosin
Chloramphenicol

Figure 5, figure supplement 1

A

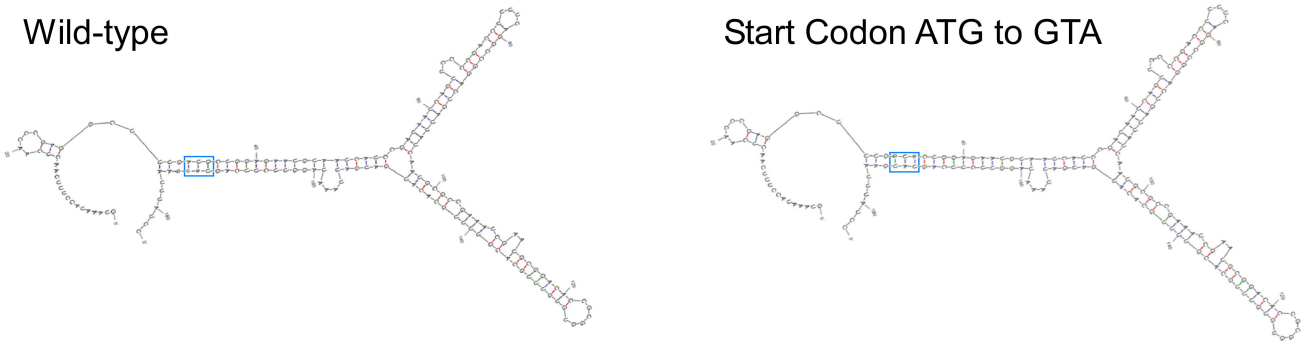

B

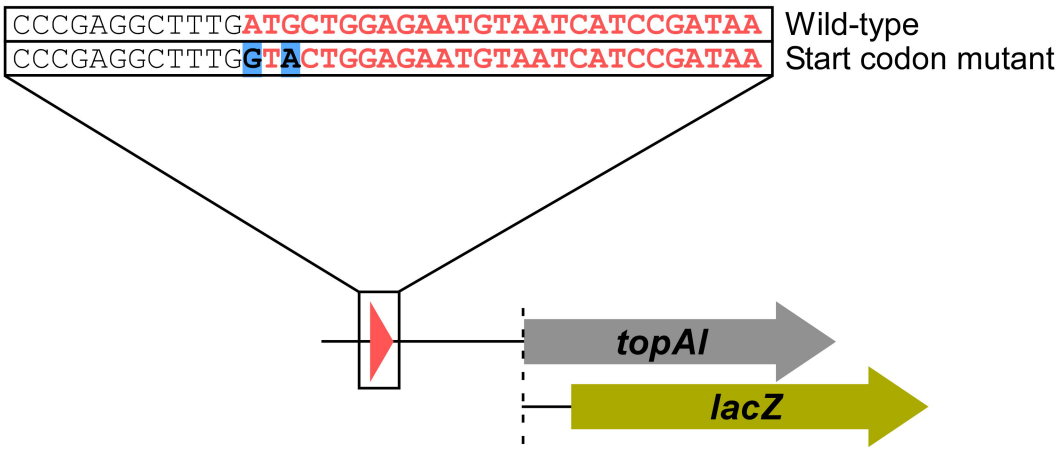

C

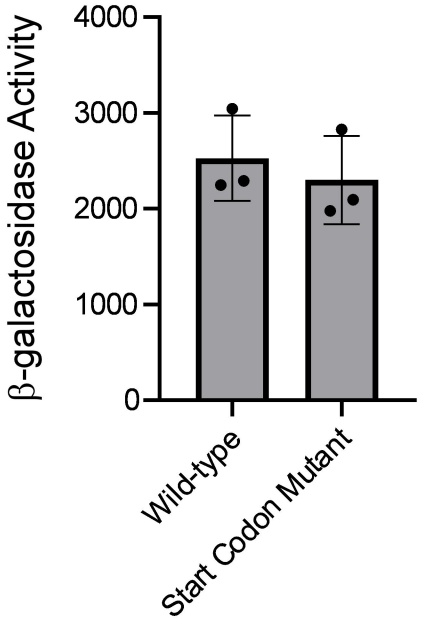

Figure 6

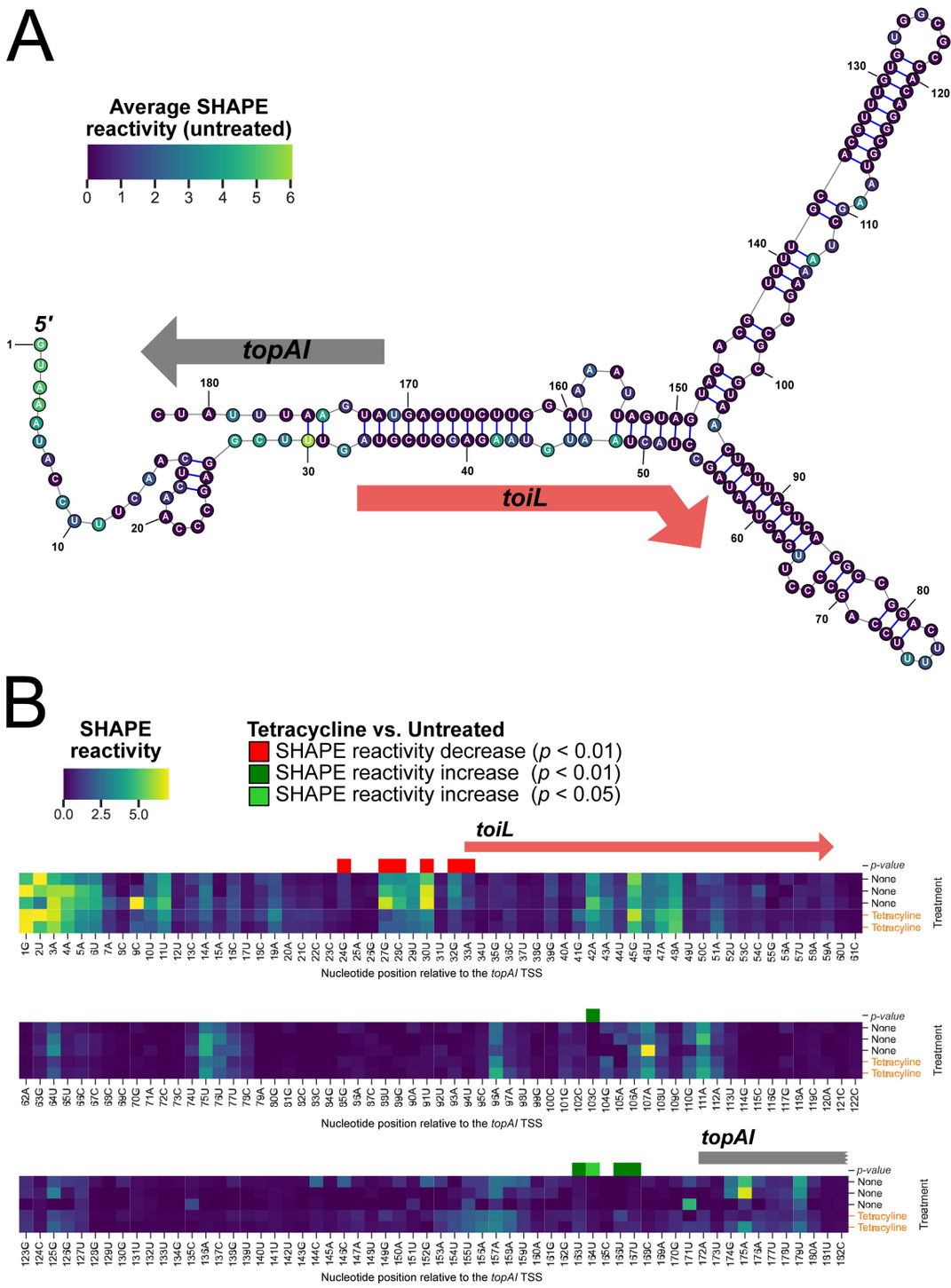
A
Average SHAPE reactivity (untreated)
0 1 2 3 4 5 6
5′
topAI
toiL
B
SHAPE reactivity
0.0 2.5 5.0
Tetracycline vs. Untreated
SHAPE reactivity decrease (p < 0.01)
SHAPE reactivity increase (p < 0.01)
SHAPE reactivity increase (p < 0.05)
toiL
p-value
None
None
None
Tetracyline
Tetracyline
Treatment
Nucleotide position relative to the topAI TSS
topAI

Figure 6, figure supplement 1

A

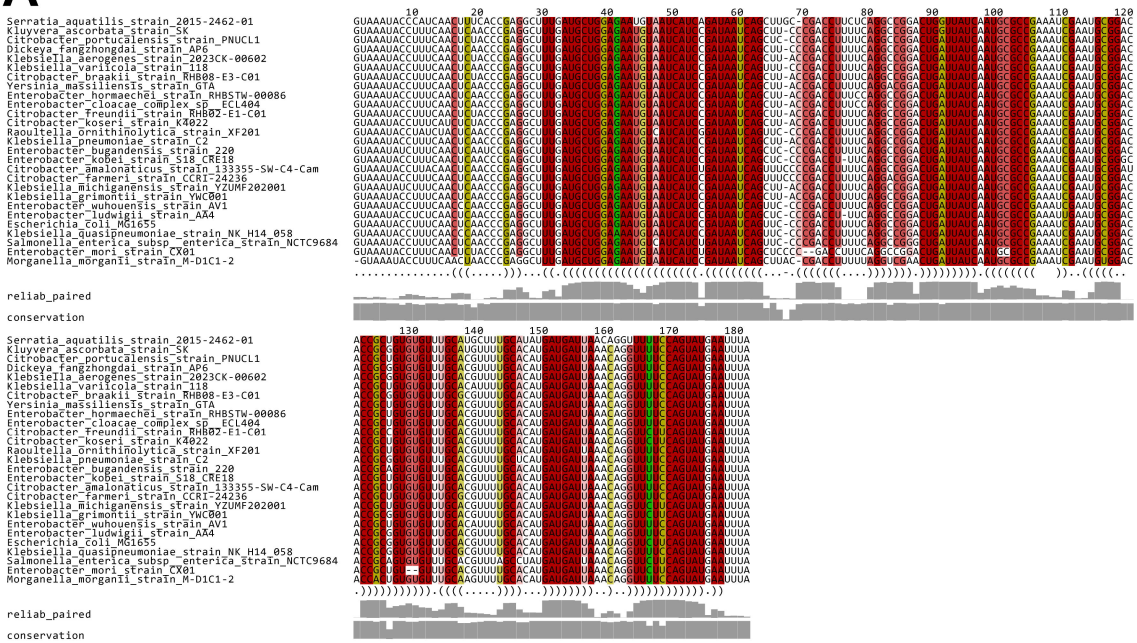

B

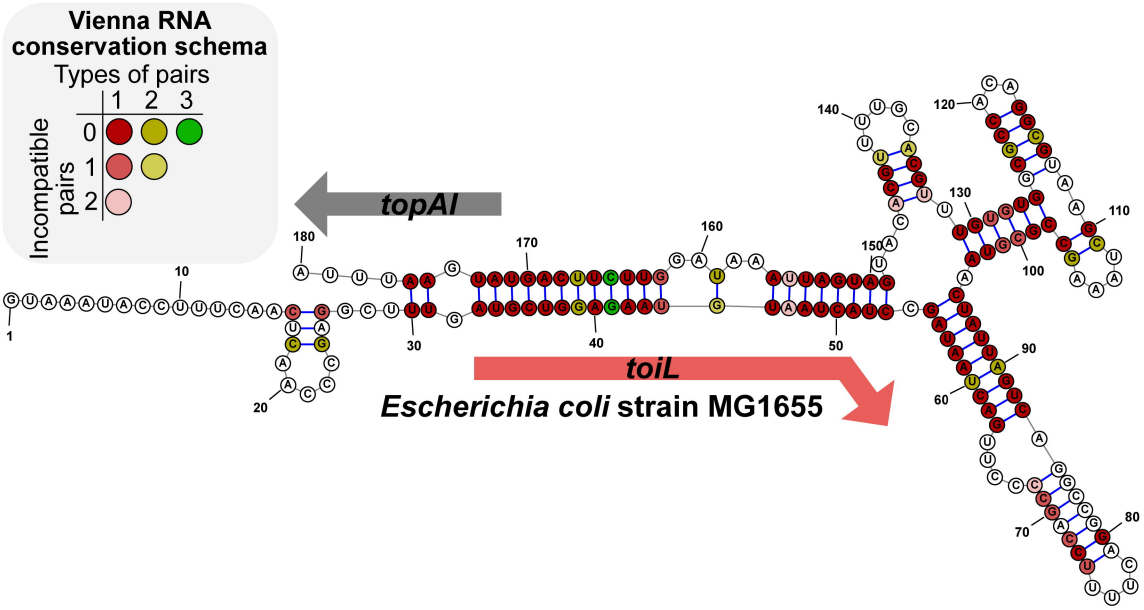

Figure 7

A

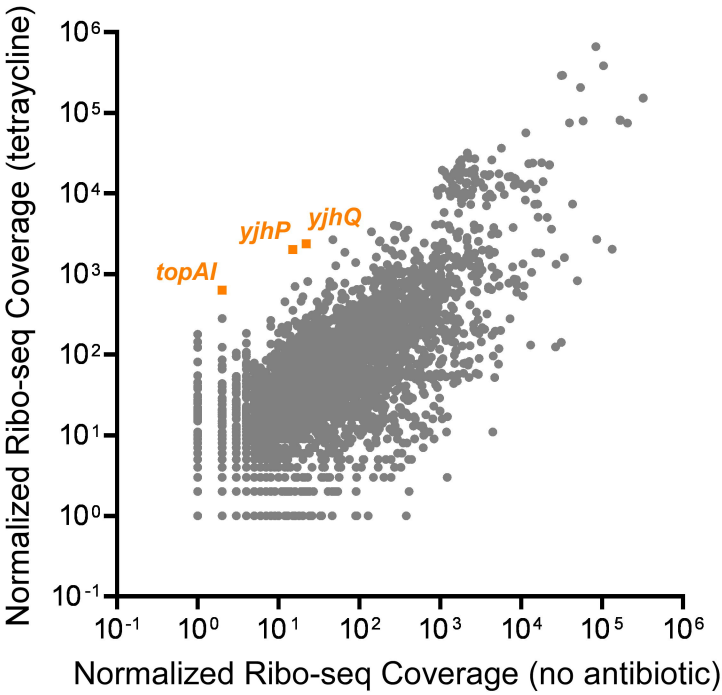
Normalized Ribo-seq Coverage (tetracycline)
Normalized Ribo-seq Coverage (no antibiotic)
topAI
yjhP
yjhQ

B

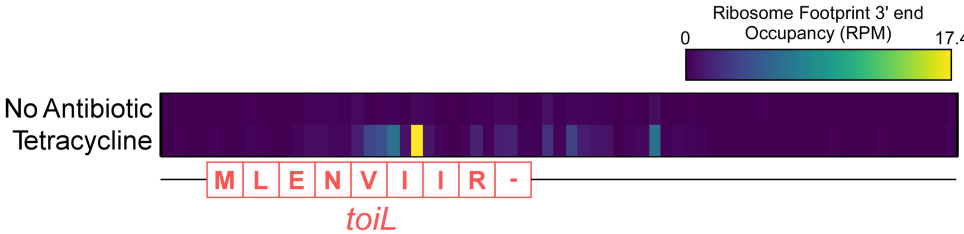
Ribosome Footprint 3' end
Occupancy (RPM)
0
17.4
No Antibiotic
Tetracycline
M L E N V I I R -
toiL

C

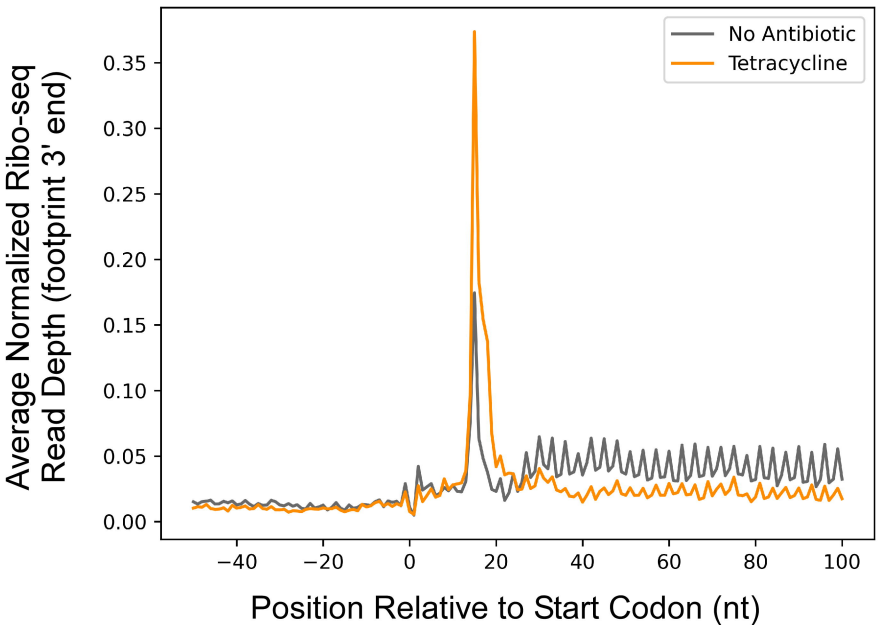
No Antibiotic
Tetracycline
Average Normalized Ribo-seq
Read Depth (footprint 3' end)
Position Relative to Start Codon (nt)

Figure 8

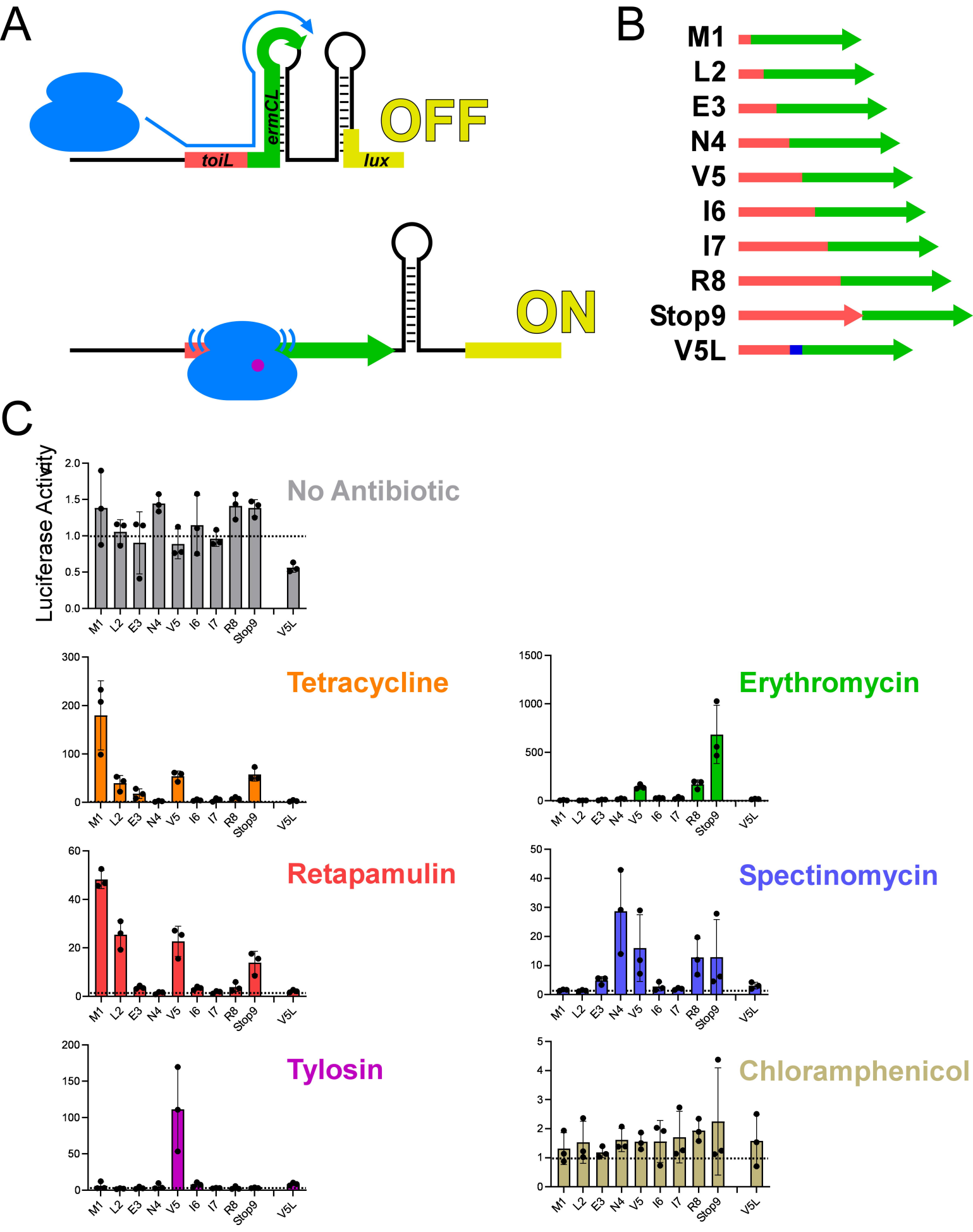
A
ermCL
toiL
lux
OFF
ON
B
M1
L2
E3
N4
V5
I6
I7
R8
Stop9
V5L
C
Luciferase Activity
No Antibiotic
Tetracycline
Erythromycin
Retapamulin
Spectinomycin
Tylosin
Chloramphenicol

Figure 8, figure supplement 1

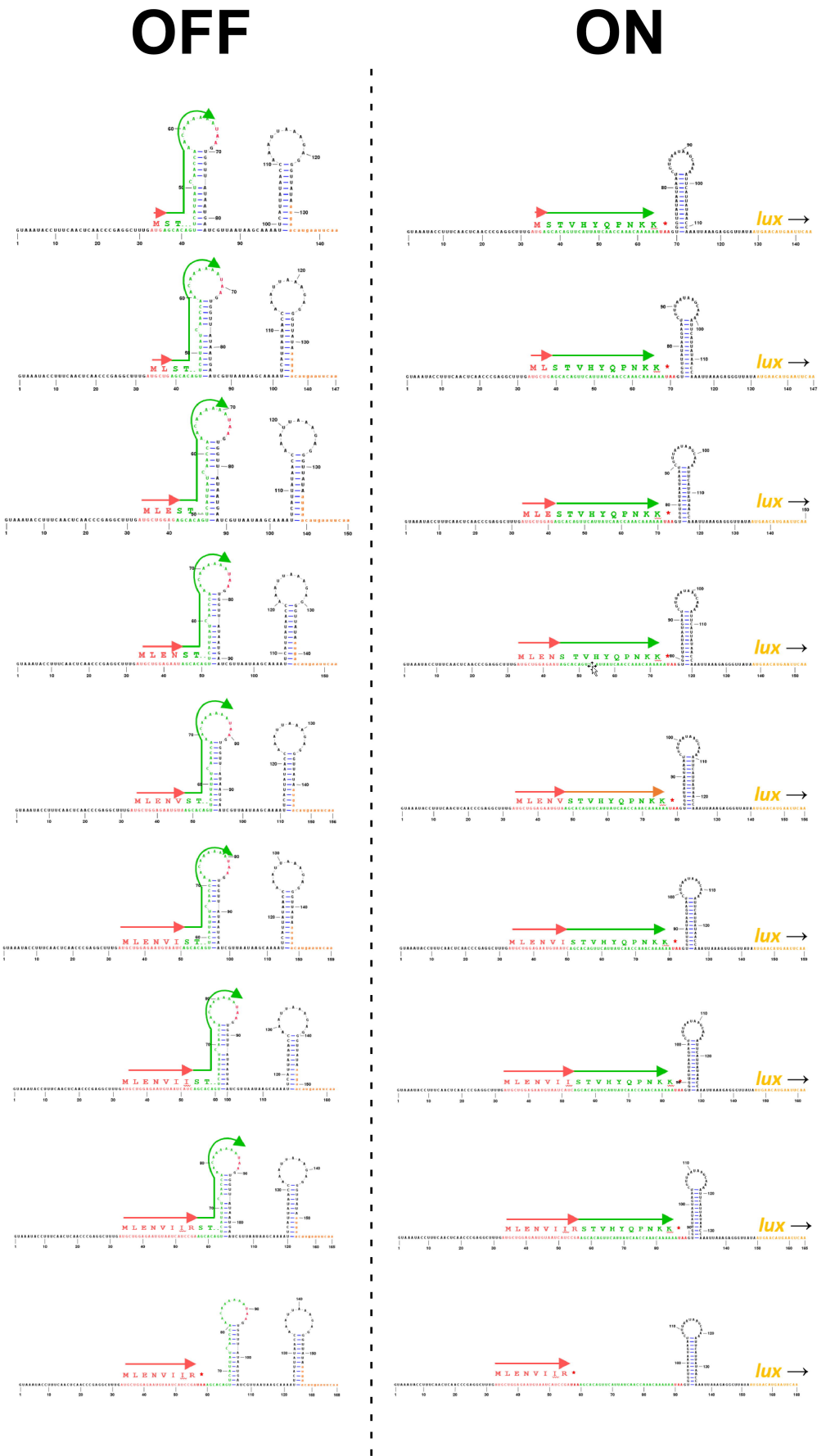

Figure 8, figure supplement 2

A

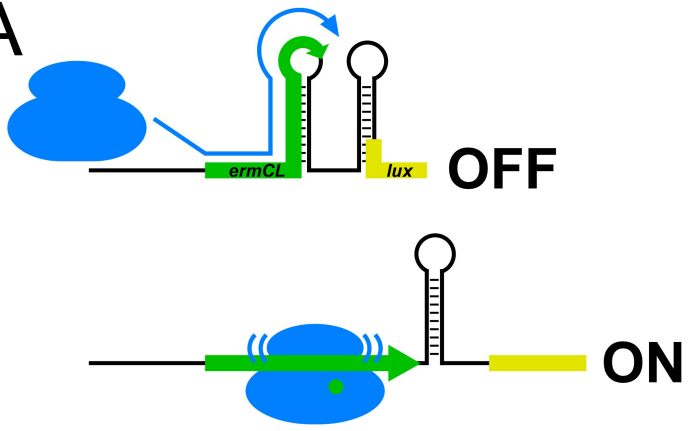

B

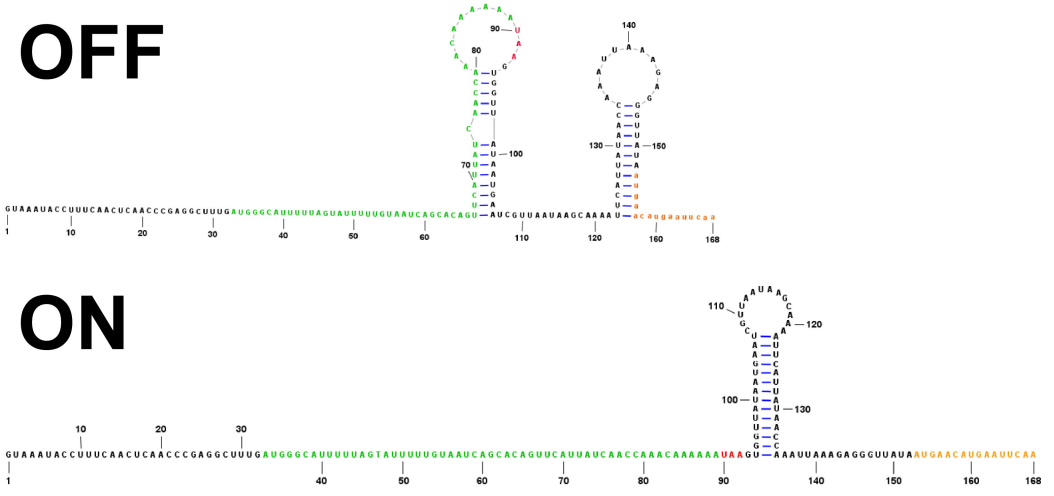

C

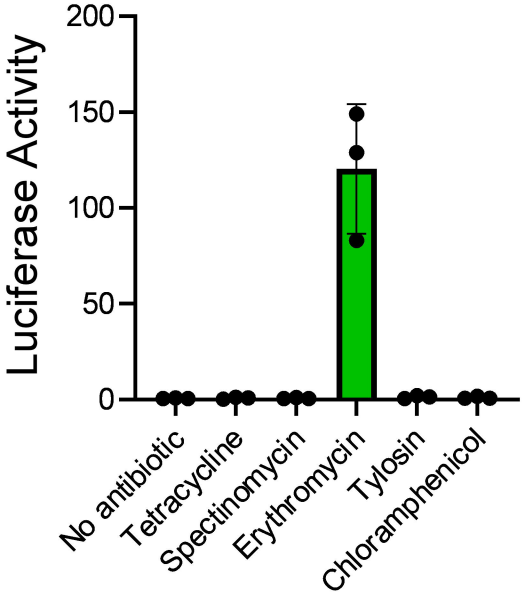

Figure 9

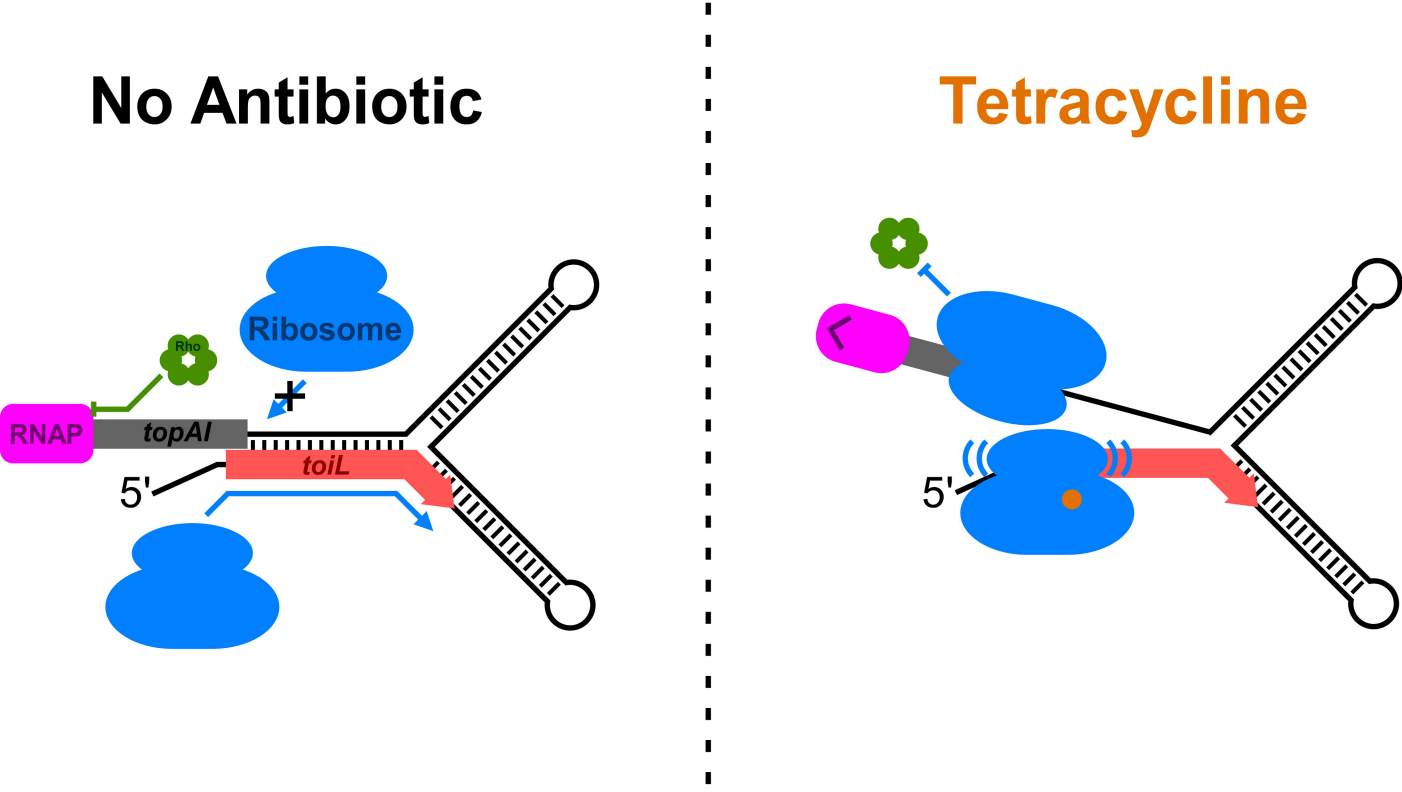
No Antibiotic
Tetracycline
Ribosome
Rho
RNAP
topAI
toiL
5'
5'